EFFECTIVE FRACTURE GEOMETRY OBTAINED WITH LARGE WATER

SAND RATIO

A Thesis

by

AMRENDRA KUMAR

Submitted to the Office of Graduate Studies of
Texas A&M University
in partial fulfillment of the requirements for the degree of

MASTER OF SCIENCE

December 2008

Major Subject: Petroleum Engineering

EFFECTIVE FRACTURE GEOMETRY OBTAINED WITH LARGE WATER

SAND RATIO

A Thesis

by

AMRENDRA KUMAR

Submitted to the Office of Graduate Studies of
Texas A&M University
in partial fulfillment of the requirements for the degree of

MASTER OF SCIENCE

Approved by:

Chair of Committee,	Peter P. Valkó
Committee Members,	Christine Ehlig-Economides
	Jean-Luc Guermond
Head of Department,	Stephen A. Holditch

December 2008

Major Subject: Petroleum Engineering

ABSTRACT

Effective Fracture Geometry Obtained with Large Water Sand Ratio.

(December 2008)

Amrendra Kumar, B.Tech., Indian School of Mines

Chair of Advisory Committee: Dr. Peter P. Valkó

Shale gas formation exhibits some unusual reservoir characteristics: nano-darcy matrix permeability, presence of natural fractures and gas storage on the matrix surface that makes it unique in many ways. It's difficult to design an optimum fracture treatment for such formation and even more difficult is to describe production behavior using a reservoir model. So far homogeneous, two wing fracture, and natural fracture models have been used for this purpose without much success. Micro seismic mapping technique is used to measure the fracture propagation in real time. This measurement in naturally fractured shale formation suggests a growth of fracture network instead of a traditional two wing fractures. There is an industry wise consensus that fracture network plays an important role in determining the well productivity of such formations. A well with high density of fracture networks supposed to have better productivity.

Shale formations have also exhibited production pattern which is very different from conventional or tight gas reservoir. Initial flow period is marked by steep decline in production while the late time production exhibits a slow decline. One of the arguments put for this behavior is linear flow from a bi-wing fractured well at early time and contribution of adsorbed gas in production at late time.

However, bi-wing fracture geometry is not supported by the micro-seismic observation. A realistic model should include both the fracture network and adsorbed gas property.

In this research we have proposed a new Power Law Permability model to simulate fluid flow from hydraulically fractured Shale formation. This model was first described by Valko & Fnu (2002) and used for analyzing acid treatment jobs. The key idea of this model is to use a power law permeability function that varies with the radial distance from well bore. Scaling exponent of this power law function has been named power law index. The permeability function has also been termed as secondary permeability.

This work introduces the method of Laplace solution to solve the problem of transient and pseudo steady-state flow in a fracture network. Development and validation of this method and its extension to predict the pressure (and production) behaviour of fracture network were made using a novel technic. Pressure solution was then combined with material balance through productivity index to make production forecast.

Reservoir rock volume affected by the fracture stimulation treatment that contributes in the production is called effective stimulated volume. This represents the extent of fracture network in this case. Barnett shale formation is a naturally fractured shale reservoir in Fort Worth basin. Several production wells from this formation was analysed using Power Law Model and it was found that wells productivity are highly dependent on stimulated volume. Apparently the wells flow under pseudo steady state for most part of their producing life and the effect of boundary on production is evident in as soon as one months of production. Due to

short period of transient flow production from Barnett formations is expected to be largely independent of the relative distribution of permeability and highly dependent on the stimulated area and induced secondary permeability. However, an indirect relationship between permeability distribution and production rate is observed. A well with low power law index shows a better (more even) secondary permeability distribution in spatial direction, larger stimulated volume and better production.

A comparative analysis between the new model and traditional fracture model was made. It was found that both models can be used successfully for history matching and production forecasting from hydraulically fractured shale gas formation.

ACKNOWLEDGEMENTS

NOMENCLATURE

n   Power Law Index

R_e Drainage Radius

r_w Wellbore Radius

J_d Dimensionless Productivity Index

J   Productivity Index

k_r Secondary Permeability

k_w Well bore Permeability

k_∞ Matrix Permeability

BHP   Bottom Hole Pressure

THP   Tubing Head Pressure

ERH   Equivalent Radial Homogeneous

PSS   Pseudo Steady State

ρ Fluid Density

Φ Porosity

c   Fluid Compressibility

c_f Formation Compressibility

c_t Total Compressibility

μ Viscosity

p   Pressure

$\vec{u}$ Velocity

m(p)   Pseudo-Pressure

z   Compressibility Factor

t	Time
M	Molecular Weight
R	Gas Constant
T	Temperature
P_i	Initial Reservoir Pressure
q	Flow Rate
q_{sc}	Flow Rate at Standard Condition
B	Formation Volume Factor
B_g	Formation Gas Volume Factor
G_p	Cumulative Production
S_{wi}	Irreducible Water Saturation
A	Area
h	Formation Thickness
t_{DA}	Dimensionless Time with Respect to Area
q_D	Dimensionless Flow Rate
Q_D	Dimensionless Cumulative Volume
r_{De}	Dimensionless Drainage Volume
mmscf	Million Metric Standard Cubic Feet

TABLE OF CONTENTS

Page

LIST OF FIGURES

FIGURE   Page

LIST OF TABLES

1   INTRODUCTION

1.1   The Importance of This Research

All the existing conventional hydrocarbon reservoirs are depleting fast and new discoveries made are decreasing in numbers and sizes. To fill the gap between consumption and production the United State shifted its focus from conventional to unconventional reservoirs to produce gas. One of the focus areas has been the gas shale reservoirs since the 80s. As a result, five shale gas plays are in production today. Technology has played a big role in the development of these fields. A comparative analysis of these shale formations has also revealed that they are widely varied in nature and each of them needs a unique technology for exploitation (Hill & Nelson, 2000)[1]. Nonetheless all of them share two very important common features — the presence of natural fractures and the need of hydraulic fracture treatments for commercial production.

Latest in the series of these gas plays is Barnett Shale in the Fort Worth basin. The geology of Barnett has been discussed in various technical papers. An overview was given by Kuuskraa[2]. The Barnett formation is a hydrocarbon rich shale rock of Mississippian age. The reservoir is highly heterogeneous in nature. Geological setting of Barnett shale from bottom to top is: Water bearing Ellenberger dolomite, Viola Simpson limestone, Lower Barnett Shale, Forestburg lime, Upper Barnett shale Marbell Falls. The lower Barnett shale is more productive than upper one. Natural

_____
This thesis follows the style and format of the *SPE Journal*.

fracture in Barnett shale is oriented in NW-SE direction and the induced hydraulic fracture tends to grow in NE-SW direction[3].

Gases are stored in shale in three different ways. Gas in the pore spaces as free gas, gas adsorbed on rock surface, and gas stored in natural fractures as free gas. Barnett is mainly a dry gas reservoir with 20% of the total gas in place is in adsorbed state which could only be produced when pressure falls below 1000 psi.

Initially only vertical wells and cross linked gel fuid were used in Barnett shale formation but the trend has changed in last 2-3 years. Vertical wells were replaced with horizontal wells and high water sand ratio took the place of high sand laden gel fluid. These changes in a way have revolutionized the production from Barnett shale formation. But this success has been a result of trial and error procedure rather than a decision based on sound engineering analysis. Optimum fracture design is still illusive for Barnett Shale due to complexity of the formation. The development of Barnett shale field can be summarized in different time frame as:

1981-1991   Research & Development Phase

1992-1997   Exploitation with cross-linked gel fracture fluid

1998-2002   Slick water and Vertical wells

2003-2006   Horizontal wells

Various attempts to correlate the effective fracture geometry with treatment parameter have either been failed or still in its early stage of development. Given the complexity of the problem, a solution is not expected by rock mechanics study any time soon. In absence of a solid rock science the first step towards the understanding of fracture in this formation would be the measurement of fracture geometry either by direct or indirect method.

Fortunately we have an emerging technology: Micro seismic mapping with applications for a direct measurement of hydraulic fracture growth in real time (Fig1.1). The fundamentals of the science involved in micro seismology are very closely related to earthquake seismology. This technique measure the hypocenter of acoustic emissions caused by stress changes in rock matrix due to fluid and proppant injection. These acoustics points used to calculate width, length and height of the fracture that yields the total acoustic volume.
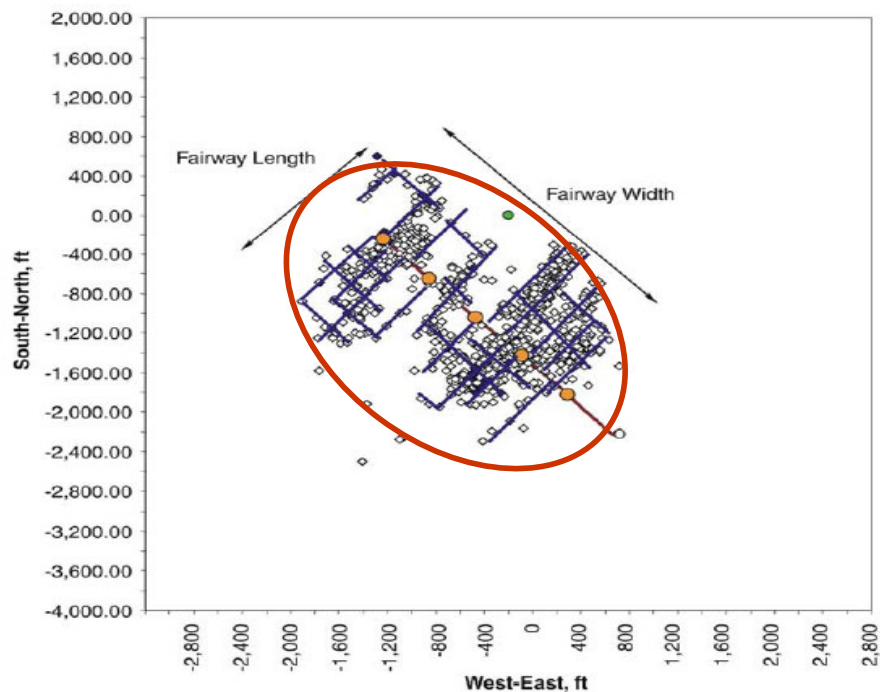
Fig 1.1: Micro Seismic Map for a Frac Job in Barnett Shale Formation (SPE 91435)

Though use of this technology has answered some of the uncertainty regarding fracture network geometry and size it has also arose quite a few questions. One of

them is high affected fracture network width (in order of hundred of feets) obtained with high water sand ratio. It can't be explained with classical fracture theory of either PKN or KGD model. In other words, we don't know yet if the acoustic volume is the same as effective stimulated volume. One of the hypotheses given by the scientists for higher fracture network width is reopening of natural fracture and its continuous connection with induced fracture. This kind of fracture system would create a network of fracture that could mimic the geometry observed in micro seismic events.

This research is an attempt to answer some uncertainties attached with fracture geometry in the Barnett Shale and also to verify the micro seismic observation by analysis of pressure and production behavior of the wells. In this work a new model is suggested for pressure transient and production analysis for fracture-stimulated formations with the purpose of providing better agreement with observed facts – especially micro seismic information. It introduces the method of Laplace solution to solve the problem of transient and pseudo steady-state flow in a fracture network characterized by its induced permeability field. Development and validation of this method and its extension to predict the pressure (and production) behavior of dendric fracture network were made using a novel technique. This model could be a useful tool to verify the dendric nature of fracture in any shale formation. One of the striking features of this model is the use of absolutely minimum number of parameters to describe formation non-homogeneity. It would help engineers to improve fracture design for gas shale formation by correlating treatment parameters with fracture geometry. It could also be used for the production forecast from such formations.

1.2   Objectives

The project objective was to develop a new well test/production model for fracture network and use this model to analyze production from hydraulically fractured wells in Barnett shale. In the heart of this research lays a very basic question: Do we create a traditional two-wing fracture geometry intersecting pre-existing micro fractures or rather we reopen/improve a dendric network of fractures? The overall objectives of the project are:

- To develop and validate the model for pressure and production behavior of a heterogeneous formation with closed circular or infinite boundary based on the method of Laplace solution.

- To develop the methodology for prediction of the transient and pseudo steady-state productivity index.

- To combine the productivity index calculation with material balance in order to forecast production.

- To apply the new method as an optimization tool for continuous improvement of fracture treatment design in shale reservoirs.

2   NEW POWER LAW EQUATION

2.1   Problem Statement

A radial homogeneous permeability model has failed to describe the rapid decline in production seen at the beginning of flow in Barnett formation wells. Perhaps because an Equivalent Radial Homogeneous model does not represent the stimulated zone nearby the well bore. Two wing fracture or dendric network models can be used as alternatives as they mimic the near wellbore condition of fractured shale formation closely. Micoroseismic observation, in-situ stress and rock mechanical properties all strongly suggest growth of dendric fracture rather than a two wing fracture. It necessitates the use of a dendric network model to simulate the flow from Barnett shale formation wells. After analyzing various models we decided to use the power law permeability model to simulate the flow from a fracture network. This model was first described by Valko & Fnu[4] and it was used for analyzing acid treatment job. The key idea of this model is the use of a power law permeability function that varies with the radial distance from well bore.

2.2   The Method of Secondary Permeability

The hydraulic fracture geometry in a naturally fractured reservoir depends on various factors such as the angle of the natural fracture relative to the hydraulic fracture, the in-situ stress direction, the fluid pressure, the rock mechanical properties, the natural fracture conductivity, etc. Depending on the conditions, induced fracture could take the following paths [5]:

- The hydraulic fracture continues to grow on its predefined path unaffected by the presence of natural fracture,

- Fracture initiates on other side with offset creating branches,

- The hydraulic fracture may also follow the natural fracture for some distance and then branch off again in its preferred direction,

- Induced fracture stops growing but natural fracture opens and dilates as a result of pressure.

Fracture mapping and production analysis of stimulated wells suggest that hydraulic fracture in a naturally fractured shale formation reopens the existing natural fracture under shear load and induces new cracks under tension with some offsets. The induced crack (Red lines) connects the natural fractures (Blue lines) and creates a complex geometry of fracture network (Fig 2-1). Secondary permeability method is a simplified approach to describe such complexity by representing the combined effect of natural and induced fracture through a single permeability function. The key idea is to describe the treated formation by a radius dependent secondary permeability (power law model of permeability) field where the created secondary permeability decreases with the distance from the treated well – mimicking the production from a fractured network.
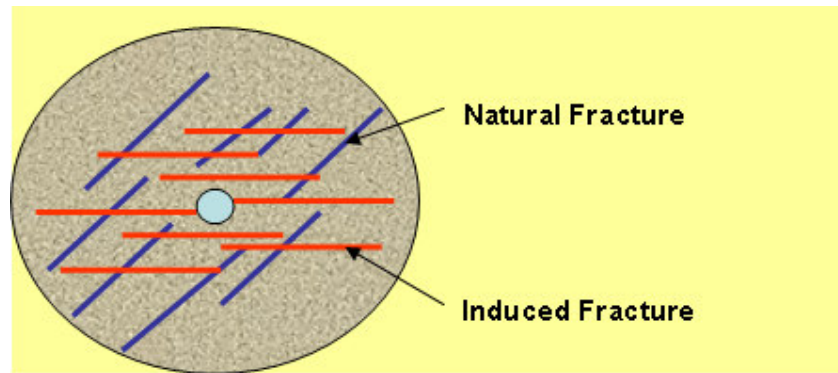
Fig 2-1 Fracture Network System

Secondary permeability can be represented by power law equation as:

$$k_r = k_w \left(\frac{r_w}{r} \right)^n \tag{2.1}$$

Where k_r is the secondary permeability at a radial distance r from well bore. At $r = r_w$ i.e. at the well bore it has the highest permeability value denoted by k_w (permeability at well bore). At $r = r_e$ the permeability is lowest and equal to the formation permeability denoted by k_∞. The rate of permeability decline depends on the power law index, n. At n = 0 well is undamaged, n < 0 implies a damaged well, and n > 0 signify a stimulated well. Effectively we have two unknown parameter: n and k_w that describes the fracture network characteristic.

Fig 2-1 shows the variation of permeability with the distance from wellbore for different n. On X-axis we have the ratio of radial distance from wellbore to wellbore radius and Y-axis represents the ratio of secondary permeability to wellbore permeability. A high value of n means sharper decline in permeability with distance.
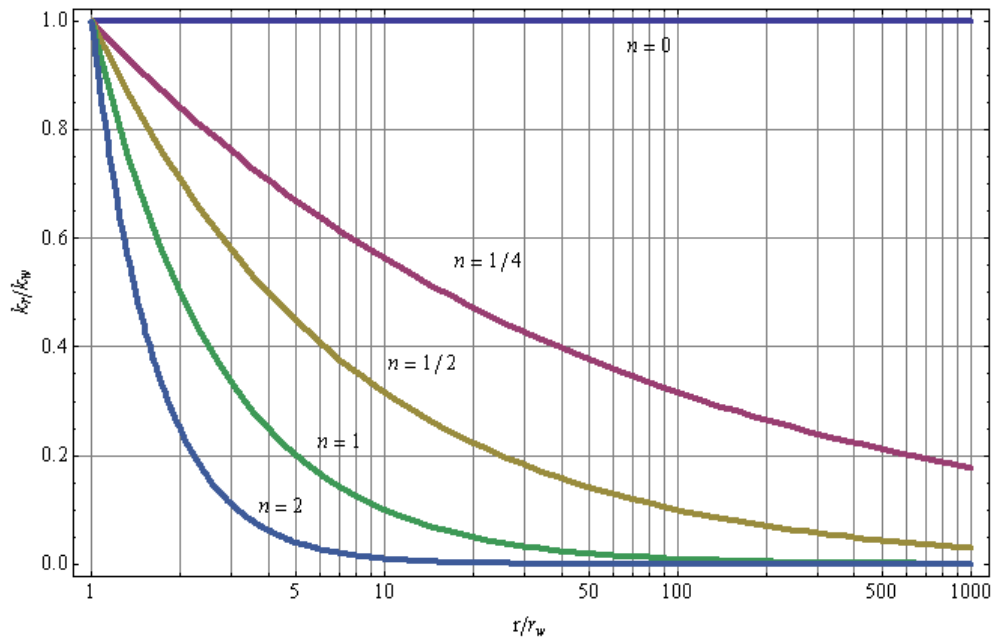
Fig 2-2 Secondary Permeability Distribution Plot for Dendric Fracture Network

2.3 Development of Equation

The diffusivity equation for fluid flow in porous media is derived by combining Darcy's law, Continuity equation, and Equation of State. This section presents the equations used to derive the diffusivity equation for power law model. Two different sets of equations have been derived, one for radial and another for composite model.

2.4 Equation of Liquid Flow

Continuity Equation:

$$\nabla \bullet \rho \vec{u} = -\frac{\partial(\phi\rho)}{\partial t} \tag{2.2}$$

Darcy's Law:

$$\vec{u} = -\frac{k}{\mu}\nabla p \tag{2.3}$$

Equation of State:

$$\rho = f(p) \tag{2.4}$$

Substituting Darcy's law in continuity equation

$$\nabla \bullet \rho\left(-\frac{k}{\mu}\nabla p\right) = -\frac{\partial(\phi\rho)}{\partial t} \tag{2.5}$$

Assuming constant μ

$$\nabla \bullet \rho k \nabla p = \mu\frac{\partial(\phi\rho)}{\partial t} \tag{2.6}$$

Differentiating LHS with ∇

$$\rho k\nabla^2 p + k(\nabla\rho)\bullet(\nabla p) + \rho(\nabla k)\bullet(\nabla p) = \mu\frac{\partial(\phi\rho)}{\partial t} \tag{2.7}$$

The density gradient $\nabla\rho$ can be written as

$$\nabla\rho = \frac{d\rho}{dp}\nabla p = \frac{d\rho}{dp}\nabla p \tag{2.8}$$

For isothermal condition liquid compressibility is

$$c = \frac{1}{\rho}\frac{d\rho}{dp} \tag{2.9}$$

Substituting Eq (2.9) in Eq(2.8) we get,

$$\nabla\rho = c\rho\nabla p \tag{2.10}$$

Substituting Eq (2.10) in Eq(2.7)

$$\rho k\nabla^2 p + kc\rho(\nabla p)\bullet(\nabla p) + \rho(\nabla k)\bullet(\nabla p) = \mu\frac{\partial(\phi\rho)}{\partial t} \tag{2.11}$$

Second term in above equation is nonlinear but it can be ignored on the grounds that c is small and the pressure gradient squared is also small. So the above equation can be modified as

$$\rho k \nabla^2 p + \rho(\nabla k) \bullet (\nabla p) = \mu \frac{\partial(\phi\rho)}{\partial t} \tag{2.12}$$

Now differentiating the right hand side

$$\rho k \nabla^2 p + \rho(\nabla k) \bullet (\nabla p) = \mu\left(\phi\frac{\partial\rho}{\partial t} + \rho\frac{\partial\phi}{\partial t}\right) \tag{2.13}$$

$$= \mu\left(\phi\frac{\partial\rho}{\partial p}\frac{\partial p}{\partial t} + \rho\frac{\partial\phi}{\partial p}\frac{\partial p}{\partial t}\right) \tag{2.14}$$

$$= \mu\left(c\phi\rho\frac{\partial p}{\partial t} + c_f\phi\rho\frac{\partial p}{\partial t}\right) \tag{2.15}$$

$$k\nabla^2 p + (\nabla k) \bullet (\nabla p) = \phi\mu c_t \frac{\partial p}{\partial t} \tag{2.16}$$

In one dimension

$$k\frac{\partial^2 p}{\partial x^2} + \left(\frac{\partial k}{\partial x}\right) \bullet \left(\frac{\partial p}{\partial x}\right) = \phi\mu c_t \frac{\partial p}{\partial t} \tag{2.17}$$

2.4.1   Equation of Gas Flow

Continuity Equation:

$$\nabla \bullet \rho\vec{u} = -\frac{\partial(\phi\rho)}{\partial t} \tag{2.18}$$

Darcy's Law:

$$\vec{u} = -\frac{k}{\mu}\nabla p \tag{2.19}$$

Equation of State:

$$\rho = \frac{pM}{zRT} \tag{2.20}$$

substituting Darcy's law and equation of state for gases in continuity equation

$$\nabla \bullet \frac{pM}{zRT}\left(-\frac{k}{\mu}\nabla p\right) = -\frac{\partial}{\partial t}\left(\phi \frac{pM}{zRT}\right) \tag{2.21}$$

for isothermal condition

$$\nabla \bullet \frac{pk}{z\mu}\nabla p = \frac{\partial}{\partial t}\left(\phi \frac{p}{z}\right) \tag{2.22}$$

expanding RHS

$$\nabla \bullet \frac{pk}{z\mu}\nabla p = \phi \frac{\partial}{\partial t}\left(\frac{p}{z}\right) + \frac{p}{z}\frac{\partial(\phi)}{\partial t} \tag{2.23}$$

$$= \phi\mu\left(\frac{z}{p}\frac{d}{dp}\left(\frac{p}{z}\right) + \frac{1}{\phi}\frac{d\phi}{dp}\right)\frac{p}{\mu z}\frac{\partial p}{\partial t} \tag{2.24}$$

This is a non-linear equation because p, μ, and z depend on the solution variable p. To solve this equation we use the concept of pseudo pressure function as following:

$$m(p) = \int_{p_b}^{p} \frac{2p}{\mu z}dp \tag{2.25}$$

$$\nabla m(p) = \frac{2p}{\mu z}\nabla p \tag{2.26}$$

$$\frac{\partial m(p)}{\partial t} = \frac{2p}{\mu z}\frac{\partial p}{\partial t} \tag{2.27}$$

where p_b is the base pressure. (14.7 psia in most states in the U.S)

The pseudo pressure is considered to be a "pseudo property" of gas because it is used as pressure (squared). Determination of the pseudo pressure at a given pressure requires knowledge of gas viscosity and z-factor as functions of pressure. As

these functions are complicated and not explicit, a numerical integration technique is frequently used.

$$\nabla \bullet k\nabla m(p) = \phi\mu(c + c_f)\frac{\partial m(p)}{\partial t} \tag{2.28}$$

$$\nabla \bullet k\nabla m(p) = \phi\mu c_t \frac{\partial m(p)}{\partial t} \tag{2.29}$$

The above equation is similar to oil equation with pressure replaced by pseudo pressure function. Following the same steps as in the case of oil phase we arrive at the final equation as

$$k\frac{\partial^2 m(p)}{\partial x^2} + \left(\frac{\partial k}{\partial x}\right) \bullet \left(\frac{\partial m(p)}{\partial x}\right) = \phi\mu c_t \frac{\partial m(p)}{\partial t} \tag{2.30}$$

2.4.2 Radial Model

Wellbore in a reservoir is most suitably described by radial geometry. In the previous section power law diffusivity equation for linear flow was derived. Above equation can be transformed into radial geometry in two easy steps.

Eq 2.17 in radial geometry can be written as

$$k\left(\frac{1}{r}\frac{\partial}{\partial r}\left(r\frac{\partial p}{\partial r}\right)\right) + \left(\frac{\partial k}{\partial r}\right) \bullet \left(\frac{\partial p}{\partial r}\right) = \phi\mu c_t \frac{\partial p}{\partial t} \tag{2.31}$$

By replacing k_r in equation 2.31 with

$$k_r = k_w \left(\frac{r_w}{r}\right)^n \tag{2.32}$$

we get,

$$\frac{r_w{}^n}{r^{n+1}} \frac{\partial}{\partial r}\left(r\frac{\partial p}{\partial r}\right) - \frac{(n+1)r_w{}^n}{r^{n+1}} \frac{\partial p}{\partial r} = \frac{\phi\mu c_t}{k_w} \frac{\partial p}{\partial t} \tag{2.33}$$

The above equation is a 2nd order, non-linear differential equation. By considering the $\frac{\phi\mu c_t}{k_w}$ independent of pressure it becomes a linear boundary value problem that can be solved with two boundaries and one initial condition.

$$p(r,0) = p_i \qquad \text{(Initial Condition)} \tag{2.34}$$

$$rk_r \left.\frac{\partial p}{\partial r}\right|_{r=r_w} = \frac{qB\mu}{2\pi h} \qquad \text{(Constant Rate Inner Boundary)} \tag{2.35}$$

$$\left.\frac{\partial p}{\partial r}\right|_{r=r_e} = 0 \qquad \text{(No Flow Outer Boundary)} \tag{2.36}$$

It is convenient to express all the equations in dimensionless form before solving. A complete derivation of dimensionless form is given in Appendix A. The Laplace transformation technique has been used to solve the Eqs 2.33 through 2.36. Laplace solution was inverted numerically using BigNumber-Stehfest[6] Algorithm to get the solution in real time domain. All the computation was done using Mathematica (Wolfram Research).[7]

A transformation technique that converts the radial geometry into equivalent linear system was also used. It facilitated fast computation and reduced the computational time considerably.

2.4.3 Composite Radial Model

A composite radial model was also developed to simulate two formations in series. Fig 2-3 illustrates the reservoir model considered for composite radial model. It shows a reservoir with two concentric circles with different permeability. In gas shale formation, inner circle may represent the dendric fracture network and outer circle the unstimulated formation.
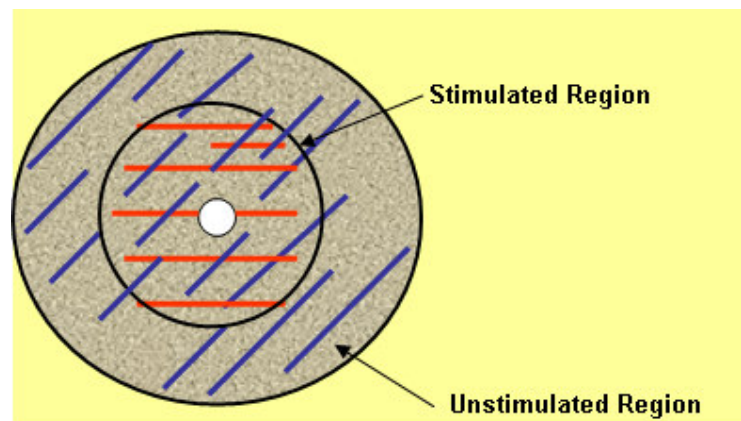
Fig 2-3 Example of Reservoir Model for Two Permeability Zone

The following system of equation was used to model the composite system.

$$\frac{1}{r}\frac{\partial}{\partial r}(k_r r \frac{\partial p_1}{\partial r}) = \phi\mu c_t \frac{\partial p_1}{\partial t} \tag{2.34}$$

$$\frac{1}{r}\frac{\partial}{\partial r}(k_f r \frac{\partial p_2}{\partial r}) = \phi\mu c_t \frac{\partial p_2}{\partial t} \tag{2.35}$$

The same technique as the radial model was used to solve above equations. A complete derivation of dimensionless form, initial and boundary conditions and pressure solution under Laplace domain is given in Appendix B.

2.5   Flow Regime Identification

Modern well test interpretation techniques extensively use the identification of flow regimes by plotting pressure and pressure derivative solution for constant rate flow on a log-log plot.[8] A number of flow regimes can be identified using this technique. The most common ones are infinite acting radial flow regime (zero slope of derivative) and pseudo-steady state flow (unit slope of derivative).

An analysis of derivative plot of power law solution reveals that there is no zero slopes line during infinite acting radial flow regime (Fig 2-4). This is because average effective permeability of formation continuously changes as the transient effect moves away from well bore. Zero slope derivative line is only valid for constant permeability. A continuously decreasing permeability gives a positive slope of 1/3 for n = 1 (Fig 2-4). The magnitude of slope is essentially a function of power law index, n. A larger slope indicates a steep decline in permeability and vice versa. For a hydraulically fracture shale gas formation, a high slope will refer to poor stimulation. However variable permeability is not the only attribute that can cause this effect. The same trend could be seen if fluid properties changes with time or space or both. We can quantify the effect of one variable if the effect of other parameter is known.

At late time, depending on the permeability distribution and drainage radius, PSS flow would be seen, identified by a unit slope derivative line. During PSS flow average permeability, porosity, net thickness, shape factor are all interchangeable so permeability function can't be uniquely determined. The dimensionless time at which transient flow changes to PSS flow will depends upon the drainage radius and power law index.
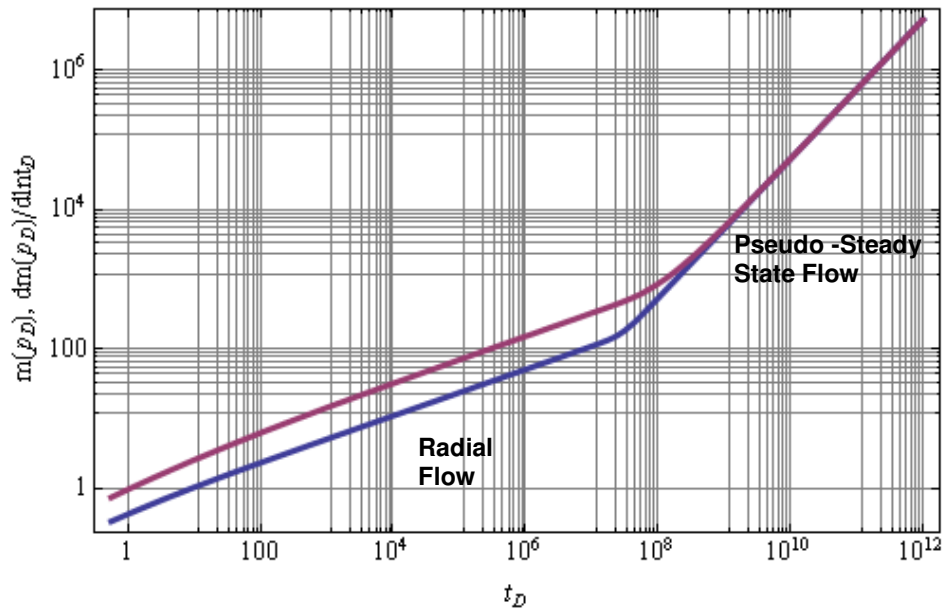
Fig 2-4 Example of Well Test Derivative Plot for Fracture Network, n>0

Well-testing Plot
Pseudo-steady State J_D: 0.000621
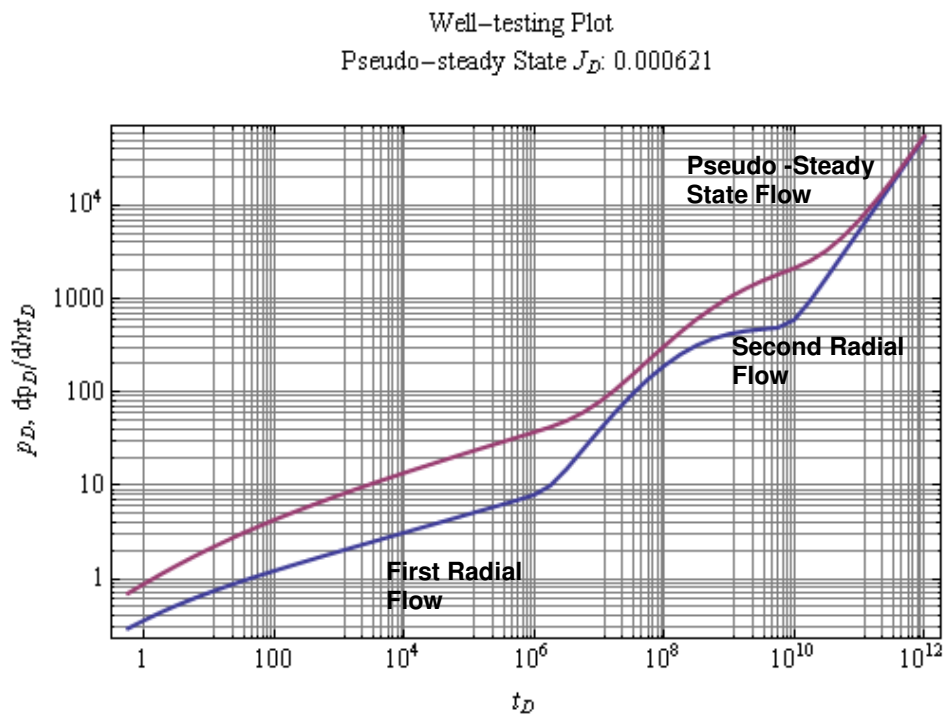
Fig 2-5 Example of Well Test Derivative Plot for Composite Formation

Fig 2-5 shows the pressure and its derivative for a composite radial model. For this calculation following input was used: Outer radius = 2000ft, Inner Radius = 200ft, Permeability Ratio = 1000, and n=1/2. Two distinct radial flow regimes are observed; one corresponds to fracture network (power law permeability) and other to unstimulated formation (constant permeability). It is not necessary that both flow regimes will be seen in all the well test analysis.

2.6   Productivity Index

Apart from the well-test analysis, new solution can be used to predict the productivity behavior of well/fracture systems. The dimensionless productivity index for constant rate and constant pressure case can be written as.(Helmy and Wattenbarger., 1998).[9,10]

Constant Rate Productivity Index:

$$J_D = \frac{1}{p_{D,trad} - 2\pi t_{DA}} \tag{2.36}$$

$P_{D,\ trad}$ is the pressure solution obtained by solving constant rate flow case. t_{DA} is the dimensionless time with respect to area.

And Constant Pressure Productivity Index:

$$J_D = \frac{q_D}{1 - \dfrac{2Q_D}{r_{De}^2}} \tag{2.37}$$

q_D is the dimensionless production rate and Q_D is the dimensionless cumulative production rate for constant pressure flow case.

Detailed derivation of the above equations has been given in Appendix B.

Productivity indices decreases continuously in transient state and become constant in pseudo-steady state. PI for similar reservoir geometry but different power law index are different in transient state but has the identical value in pseudo-steady state. It means we can use the constant rate solution for constant pressure flow with good approximation if a well flow under pseudo-steady state for long time. In that case pseudo-steady state productivity index is a single parameter that can describe a well productivity and can be used to compare the reservoir productivity.

Effect of n on dimensionless well productivity for constant rate and constant pressure case has been compared in Fig 2-6. Dimensionless productivity index has been plotted against dimensionless time for n = 0 and 2 and drainage radius 200 ft. Higher value of n causes a larger difference in dimensionless productivity index. Difference in dimensionless PI is minimum for n = 0.
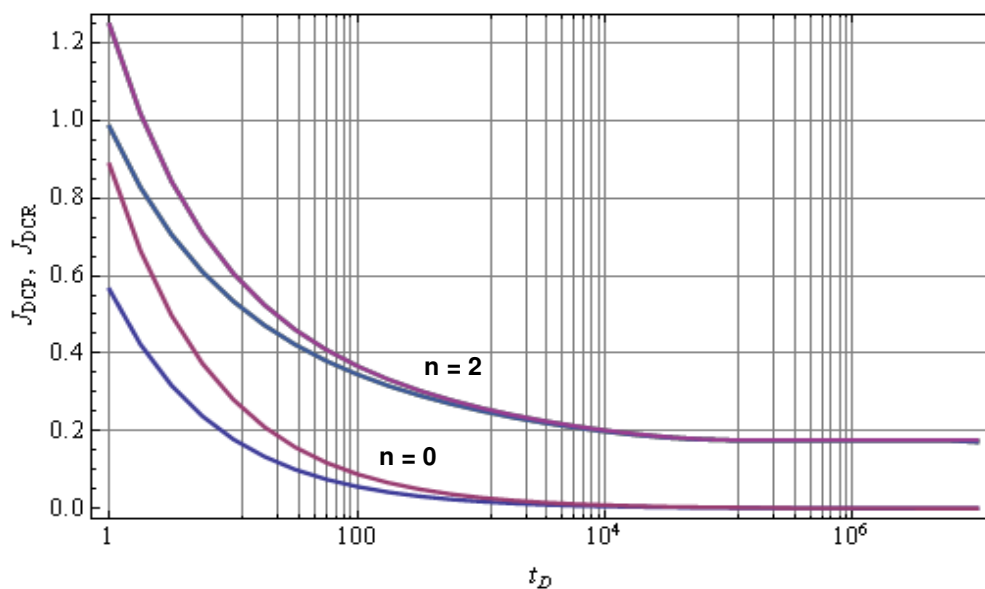
Fig 2-6 Example of J_d for Constant Rate & Constant Pressure Solution, n = 0, 2

2.7   Production Forecast

Decline curve analysis, numerical simulation, and well test analysis coupled with material balance, are few industry assortments used for production forecasting. Decline curve analysis is essentially a statistical approach to production forecasting that doesn't use any reservoir parameters. So a correlation between production potential of a reservoir and its properties can't be established with this method. Numerical simulation is the most robust and reliable method but it requires large computational capability and time to produce the result. Availability of numerical model is also an issue. Well test coupled with material balance is the best approach to a quick production forecasting. With this method, it's also possible to correlate productivity of the well with formation and identifiable fracture parameters that can further be used in optimizing fracture design.

Similar to other models power law model also requires productivity index for the whole time span of production to make a production forecast. In previous section it is already shown how the dimensionless productivity index can be determined for power law model using the dimensionless pressure solution. End of the transient flow and beginning of the pseudo-steady state flow is one of the most critical parameters that will influence production behavior of a well. Depending on the drainage radius, formation permeability and flow regime etc. transient flow could last for either a very short time (for example high permeability reservoir) or very long time (tight gas or shale reservoir).

In order to forecast production, we need to combine the productivity index with material balance. Flow from a reservoir depends on its average reservoir pressure along with other factors. Material balance relates the produced gas with the

reservoir pressure depletion giving us the important information about average reservoir pressure.

To calculate the average reservoir pressure of a gas reservoir only expansion of fluid needs to be considered. Assuming isothermal operation the average pressure equation can be given as

$$\bar{p} = \frac{p_i Z}{Z_i}\left(1 - \frac{G_p}{G_i}\right) \qquad (2.38)$$

Where G_p is the cumulative production and G_i is the initial gas in place.

Darcy's Law in modified form can be used to calculate the flow rate for dendric reservoir. Formation permeability has been replaced by well bore permeability, k_w in this modified form.

$$q_{sc} = \frac{\sqrt{k_w}\, h}{1424T} \times J_{D,t_{DA}} \times \left[m(\bar{p}) - m(p_{wf})\right] \qquad (2.39)$$

The steps followed for production forecasting is given in Table 2-1.

Table 2-1 Production Forecasting Method

1. Calculate the dimensionless pseudo pressure solving diffusivity equation.
2. Calculate the dimensionless productivity index using pseudo pressure solution. $J_{D,t_{DA}}$
3. Prepare pseudo pressure function $m(p) = \int_{p_b}^{p} \frac{2p}{\mu z} dp$
4. Specify initial pressure p_i.
5. Specify wellbore flowing pressure p_{wf}.
6. Take a time interval Δt.
7. Calculate production rate and production in the time interval. $$q_{sc} = \frac{\sqrt{k_w}\, h}{1424\, T} \times J_{D,t_{DA}} \times \left[m(\bar{p}) - m(p_{wf}) \right] \quad \text{and} \quad \Delta G_p = q_{sc} \Delta t$$
8. Apply material balance and calculate new average pressure. $\bar{p} = \frac{p_i Z}{Z_i}\left(1 - \frac{G_p}{G_i}\right)$ G_i is the original gas in place and can be calculated by using equation $G_i = \frac{Ah\phi(1 - Swi)}{B_{gi}}$
9. Repeat steps 6 –8

3   METHODOLOGY

This section presents the methodology used to determine the flow rate for constant pressure flow. Mathematica was used to solve the power law permeability diffusivity equation and for other programming purposes.

3.1   Example Calculation: Production Profile

Flow rate calculation for gas reservoir at constant bottom hole pressure is rather a straight forward approach. The steps have already been described in Section 2. Here we have shown the actual calculation at each step. Data used for this calculation is given in Table 3-1.

Table 3-1 Data for Example Case

Stimulation Index, n	**2**
Drainage Radius, R_e	**225 ft**
Well bore Radius, R_w	**0.328 ft**
Well bore Permeability, K_w	**188.225 md**
Formation Permeability, K_∞	**0.0004 md**
Thickness, h	**266 ft**
Initial Pressure, P_i	**3000 Psi**
Gas Gravity, γ_g	**0.7**
Mole fraction, N_2	**0**
Mole fraction, CO_2	**0**
Mole fraction, H_2S	**0**
Porosity, Φ	**0.05**
Water Saturation, S_w	**0.1**
V_L	**5.80E-10**
P_L	**5.22E-10**
Spec Gravity Rock, γ_s	**2.65**
BottomHole Flowing Pressure, Pwf	**500 Psi**

3.1.1 Dimensionless Pressure and Productivity Index

First of all we calculate the dimensionless pressure solving power law diffusivity equation. Fig 3-1 shows the pressure solution in the form of Bourd et el type curve using input from Table 3-1. The blue line is dimensionless pseudo pressure function and red line is the log derivative of this function.
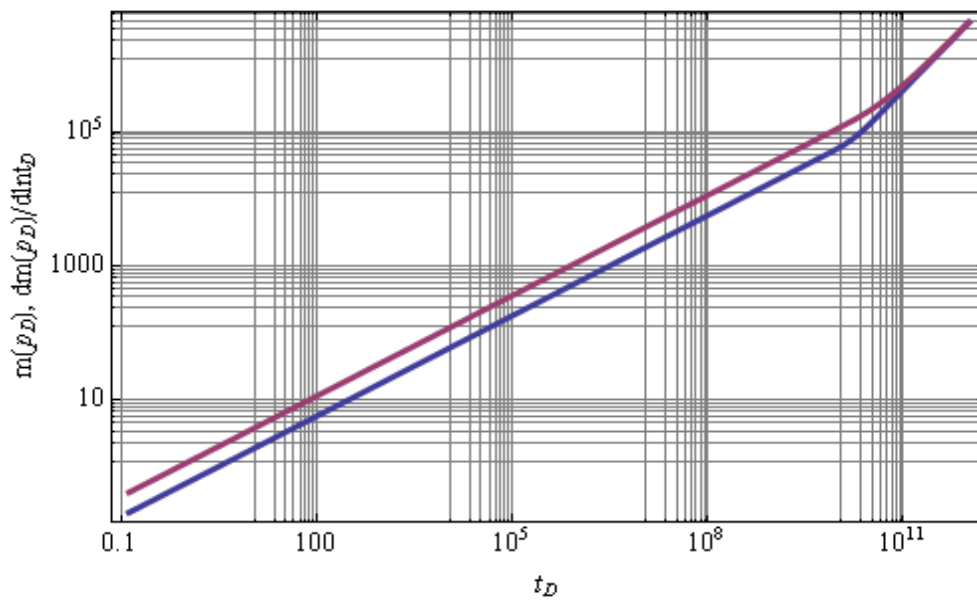
Fig 3-1 Pseudo- Pressure Derivative Plot

Using dimensionless productivity index equation for constant flow rate solution given by Helmy and Watenebrg, Fig 3-2 was plotted. It shows the Dimensionless Productivity Index vs. Dimensionless Time on a Log-Linear scale. Fig 3-3 is the same plot on Log-Log scale.
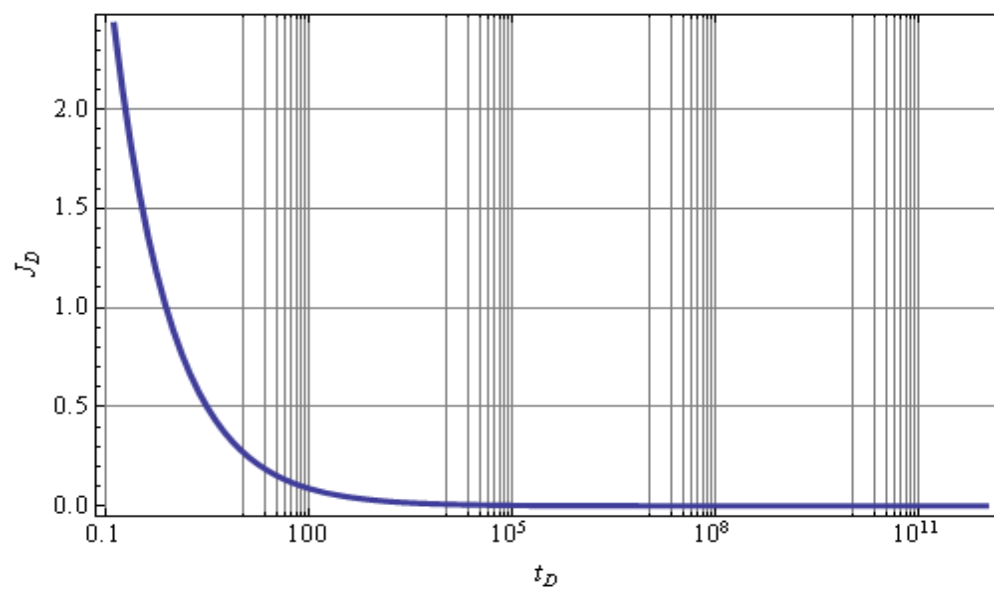
Fig 3-2 Dimensionless Productivity Index on Log-Linear Scale
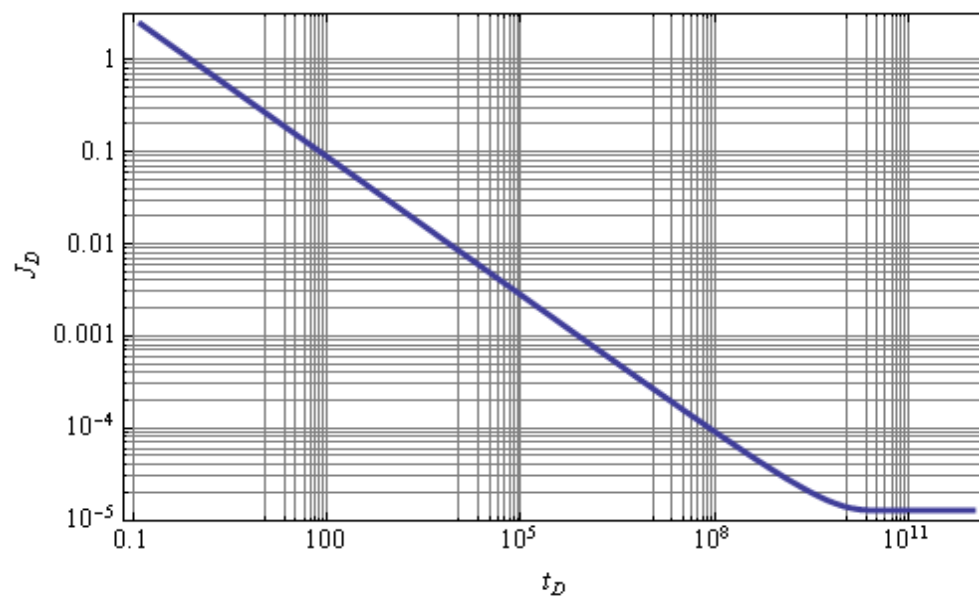
Fig 3-3 Dimensionless Productivity Index on Log-Log Scale

3.1.2 Auxiliary Curves

Gas pseudo-pressure curves are used to convert the pseudo pressure in real pressure. Adsorbed gas volume plot gives the volume of gas released with each unit reduction in reservoir pressure. These and other curves have been explained in detail in `Appendix E.

3.1.3 Production Profile Using Material Balance

Production profile is a very useful tool that helps in making economic decision and development planning. Once we calculate the productivity index and draw pseudo pressure plot it's a simple material balance calculation that produces the production profile for a constant pressure solution. Fig 3-4 shows such a production profile using input form Table 3-1. A steep decline in production in the beginning is due to power law permeability used for this model.
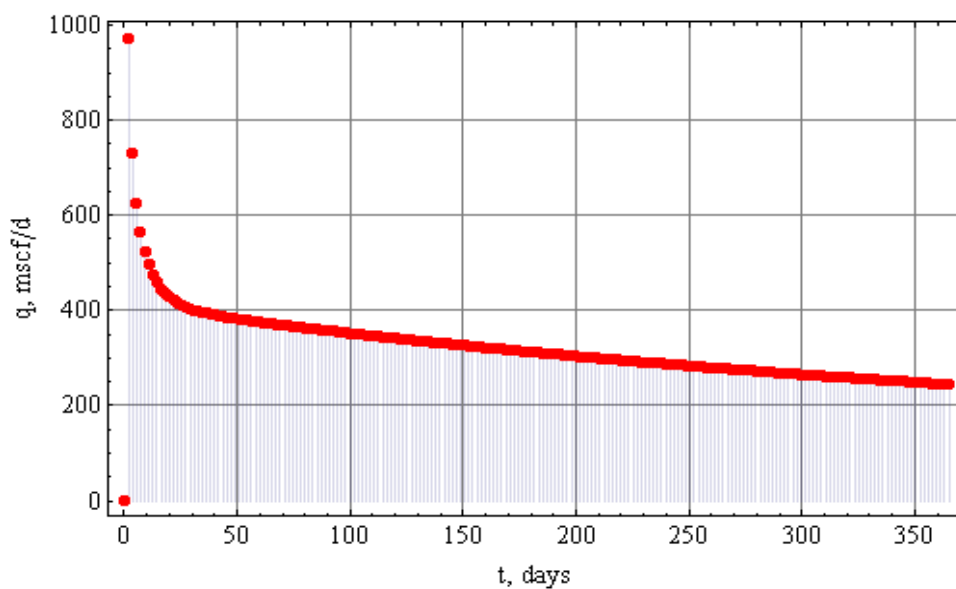
Fig 3-4 Example Well Production Profile

3.2   Model Validation

This is the first solution of its kind for power law permeability. It has not been solved by any other method in the petroleum field so we can't validate it by comparing with any other work. Nonetheless, solutions can be validated for homogeneous radial case that corresponds to n value equal to zero. Various well known solutions are available for radial homogeneous case. We choose professional software Kappa (Topaze Module)[11] to verify the results because their methodology for flow rate calculation is the same as used by this model. For non- homogeneous case (n values other than 0) model was validated by comparative analysis. The results were compared for a number of power law index and drainage radius values and validated by comparing the outputs.

3.2.1   Validation with Production Model for Radial Homogeneous Case (n = 0)

Production rate generated from new model was compared with the output from Saphir. Gas was used as hydrocarbon fluid so that pseudo pressure function can also be validated. Data used for this analysis is given in Table 3-2.

Table 3-2 Input Data for Constant Pressure Model Validation

Wellbore Radius,Rw	0.328 ft
Drainage Radius,Re	250 ft
Initial Pressure,Pi	4000 psi
Formation Thickness,h	400 ft
Permeability,k	0.01 md
Porosity,Φ	0.1
BHFP,Pwf	500 psi
Rock Compressibility,Cr	10^-6 1/psi
Gas Gravity,γg	0.7
Water Saturation, Sw	0
Temperature, T	212 F
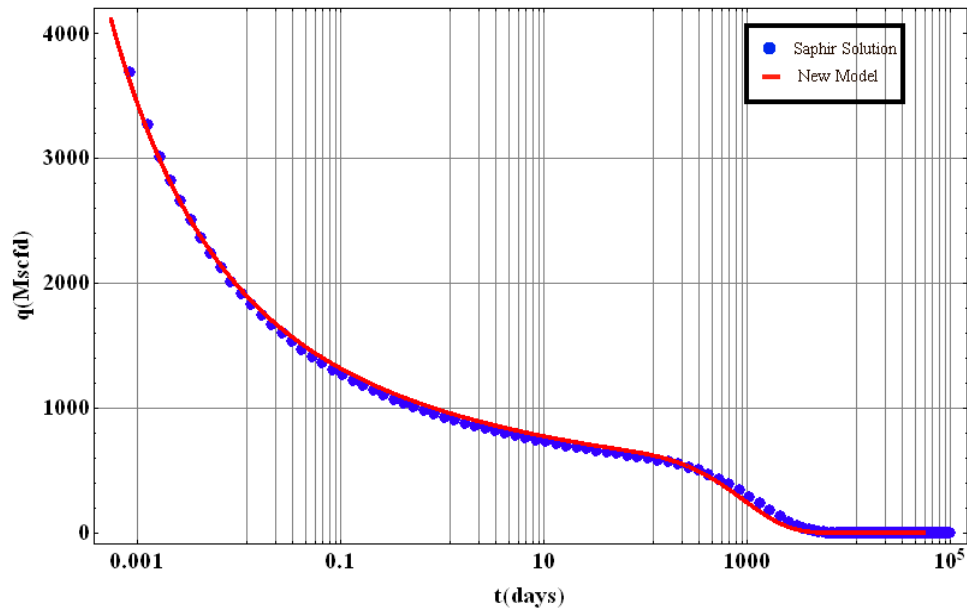
Fig 3-5 Production History Match for Constant Pressure and n = 0

In Fig 3-5, the solid blue circles show the production rate from new model. The red continuous line indicates the production rate calculated using Topaze. This graph verifies the results from new model. The slight difference observed is due to the different correlations used for viscosity and compressibility in two models.

3.2.2 Validation with Pressure Derivative Plot for Inhomogeneous Case

As said earlier, currently there is no other solution available for power law permeability model so a comparative approach was used for validation and the results are presented from Fig 3-6 to Fig 3-7. Fig 3-6 shows the sensitivity to stimulation index on pressure response for constant flow rate solution. At n = 0, pressure response is similar to a homogeneous radial model. A gradual increase in derivative pressure slope with increase in stimulation index verifies the theoretical concept. A high J_d also indicates low average formation permeability and a longer transient flow period which is evident with this plot.
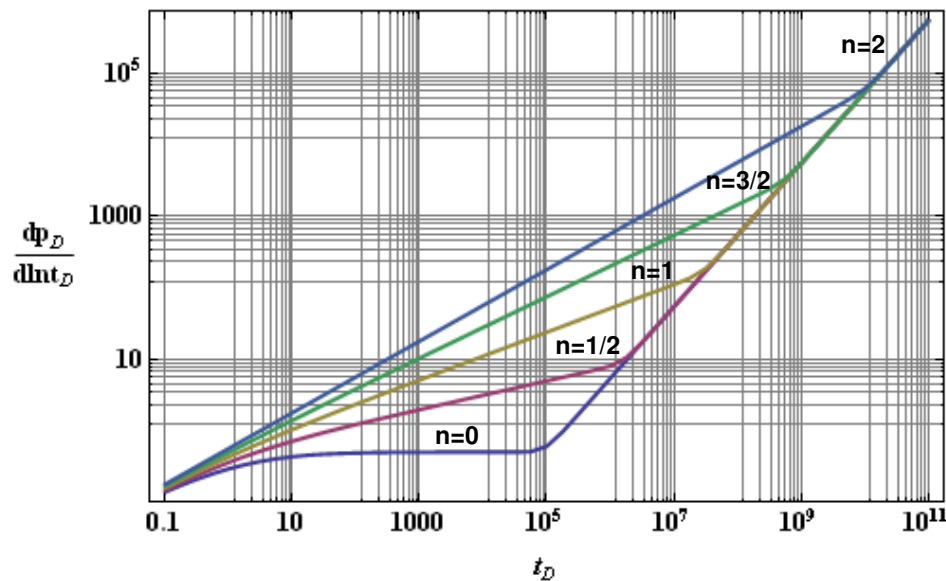
Fig 3-6 Well Test Derivative Plot: Sensitivity with n

Table 3-3 shows the approximate slope of derivative pressure for constant flow rate solution. The values are measured directly from the above plot.

Table 3-3 Pressure Derivative Slope for Different n

n	Slope
0	0
1/8	0.14
¼	0.18
3/8	0.21
½	0.24
1	0.34
3/2	0.43
2	0.50

Fig 3-7 Pressure Derivative Slope vs. Power Law Index

A correlation can also be established between Power Law Index and Pressure Derivative slope with a power law equation (Fig 3-7).

Fig 3-8 shows the sensitivity to effective stimulated radius on pressure response. The pressure derivatives response during transient state is independent of drainage radius. PSS regime starts earlier in the well with lower drainage radius.
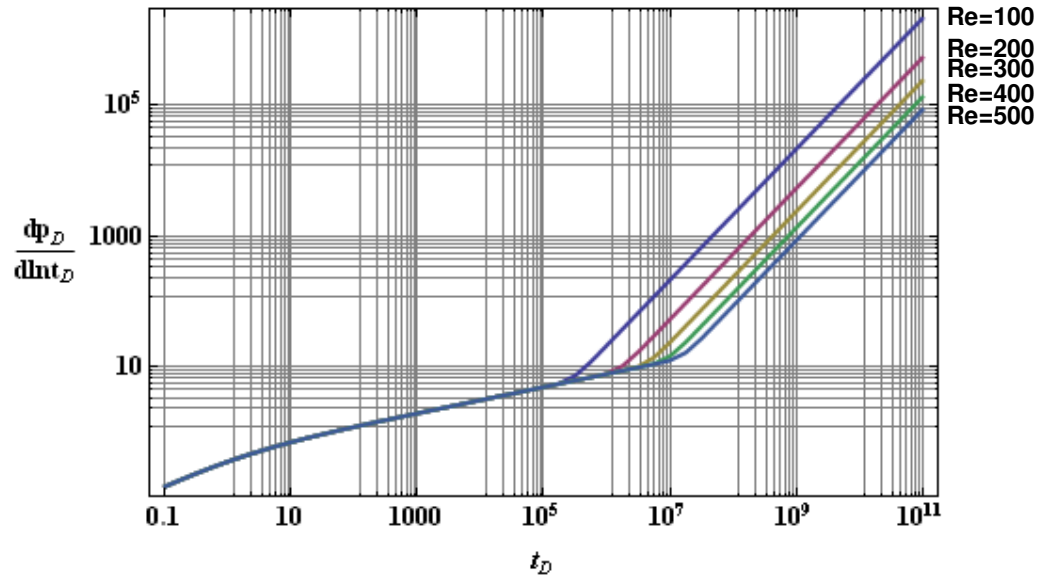
Fig 3-8 Well Test Derivative Plot: Sensitivity with Re

3.2.3 Validation with J_d for Inhomogeneous Case

Effect of variation in n and Re can also be verified with J_d plot. Fig 3-9 shows the calculated J_d for n = 0 to 2 in steps of 1/2. Transient flow last longer in formation with higher n value. By definition, start of pseudo steady state is marked by the beginning of constant J_d. One with higher n value takes more time to reach pseudo steady state.
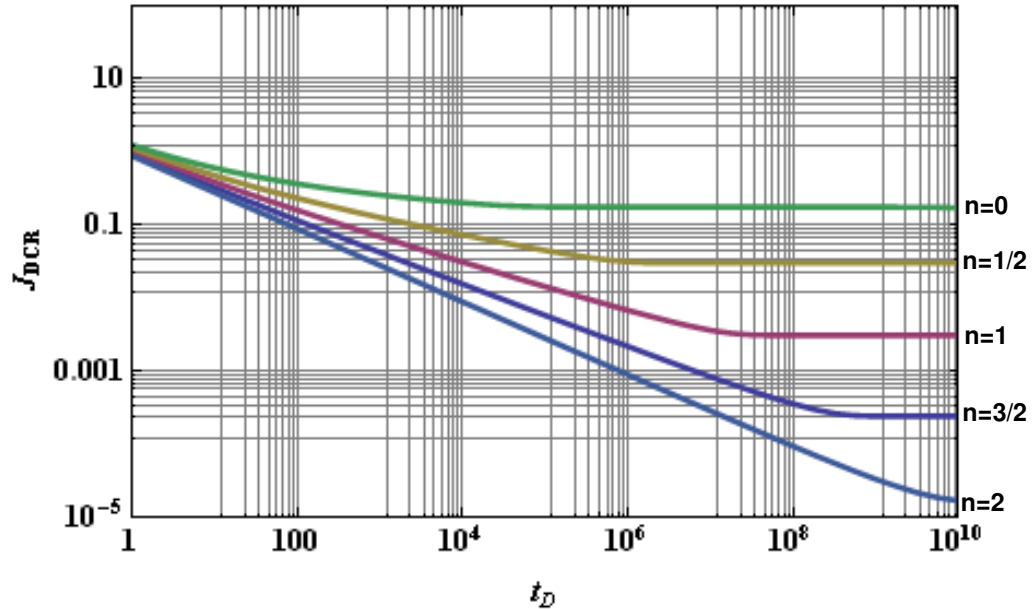
Fig 3-9 J_d Plot Sensitivity with n

Table 3-4 shows the approximate slope of dimensionless power law index for constant flow rate solution. These values are exactly same as the pressure derivative plot.

Table 3-4 Slope of J_d for Different n

n	Slope
1/8	-0.14
1/4	-0.18
3/8	-0.21
1/2	-0.24
1	-0.34
3/2	-0.43
2	-0.50

Fig 3-10 shows J_d for R_e =100 to 500 in steps of 100 at n = 2. During transient flow all the curves overlap on each other since the flow is independent of n in that period. One with the lowest value of drainage radius attends the pseudo steady state earliest.
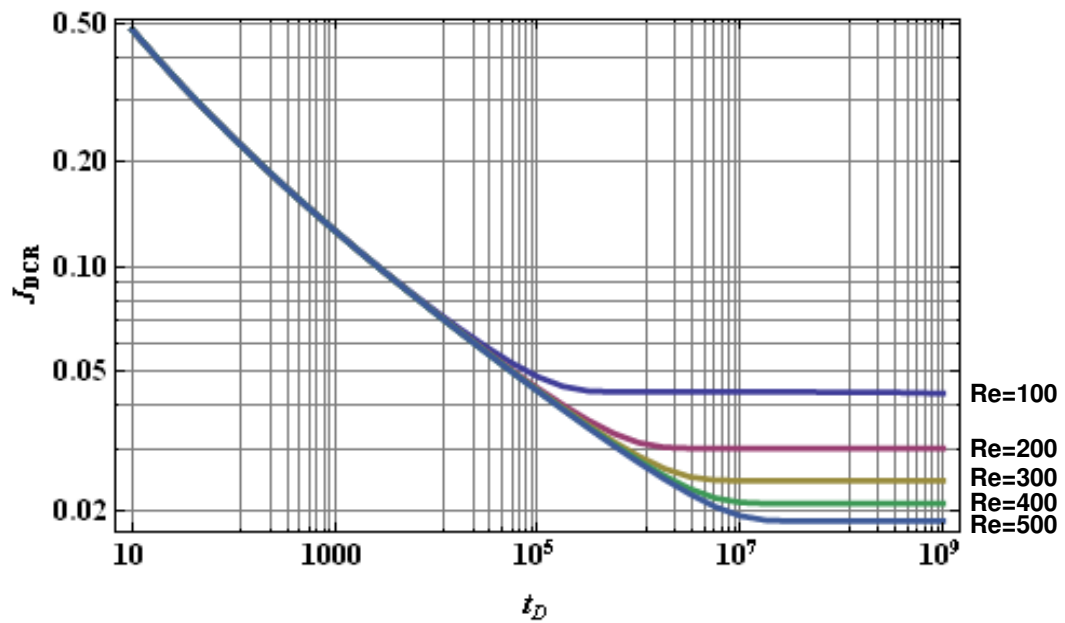
Fig 3-10 J_d Plot Sensitivity with Re

4   RESULTS AND CASE STUDIES

4.1   Data Sampling

Data for this work were collected from public database HPDI. Barnett Shale's monthly production and yearly wellhead pressure data were used for analyses. In first year majority of the wells produces at variable rate and variable pressure until the well head pressure stabilizes to flow line pressure. Since this model is restricted to the constant rate or constant pressure solution only those wells were considered for the analysis that has been producing at constant bottom hole pressure for long time. Fig 4-1 to Fig 4-4 shows the production and pressure profile for 4 such wells. These wells have produced at tubing head pressure of 300/400 psi for more than 5 years. Bottom hole pressure was calculated from tubing head pressure. Pressure losses in the well bore was calculated using standard correlations. Since the frictional losses in the well bore was not significant change in BHP with flow rate at constant THP was ignored. Well 2540773, shown in Fig 4-4, is a refracutre candidate indicated by a spiked increase in production rate.

Reservoir, fluids and rock properties were taken from the well test and stimulation report available at Rail Road Commission of Texas (RRC) website. Parameters were assumed wherever it was not known. Initial pressure was assumed constant at 3000 Psi for all the wells.
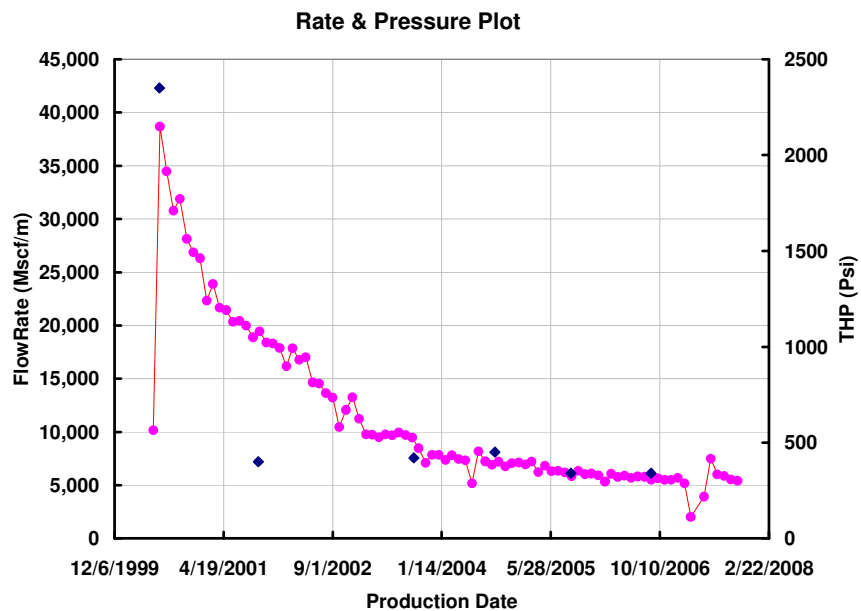
Fig 4-1 Production and Pressure Profile: Well 2540767
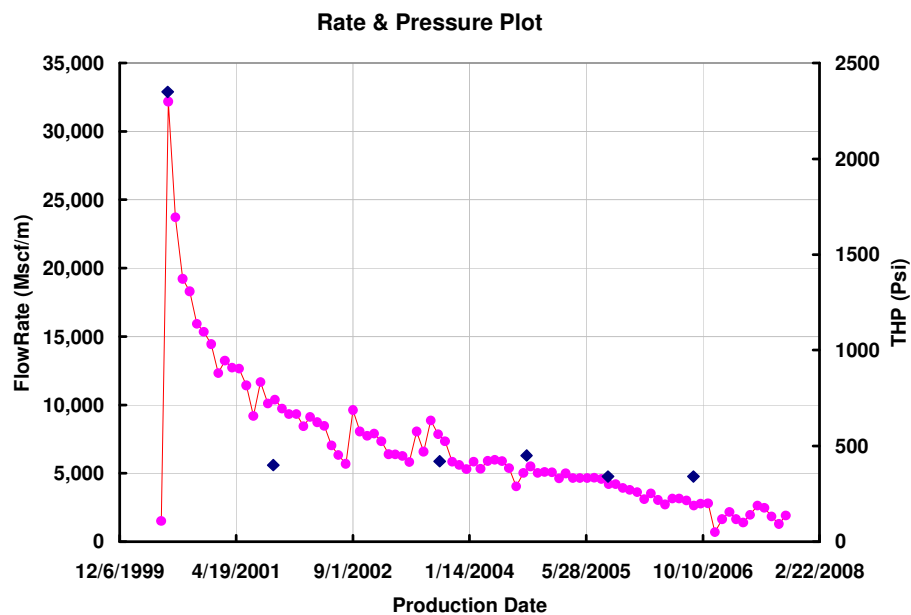
Fig 4-2 Production and Pressure Profile: Well 2540773

Rate & Pressure Plot
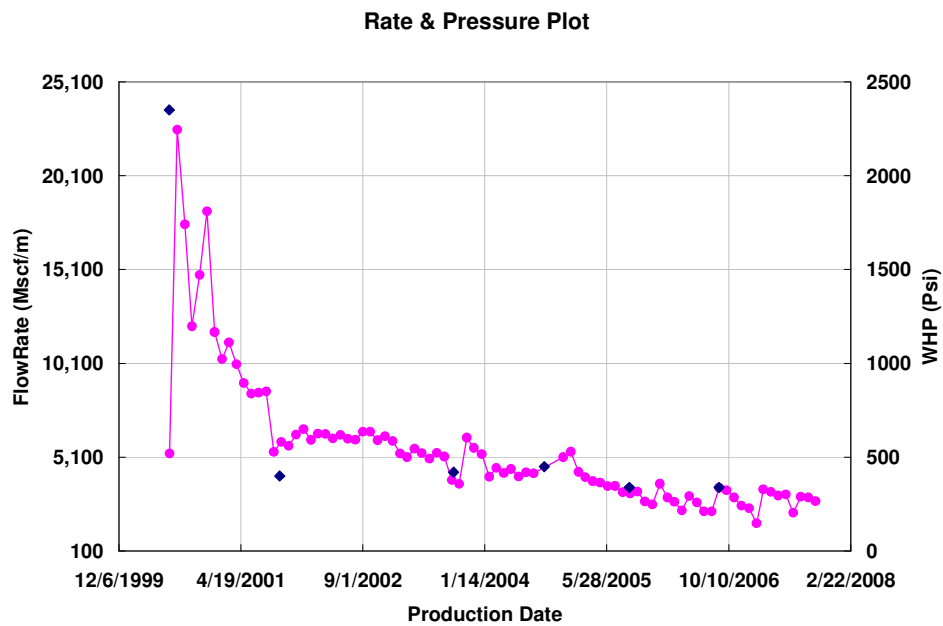
Fig 4-3 Production and Pressure Profile: Well 2540777

Rate & Pressure Plot
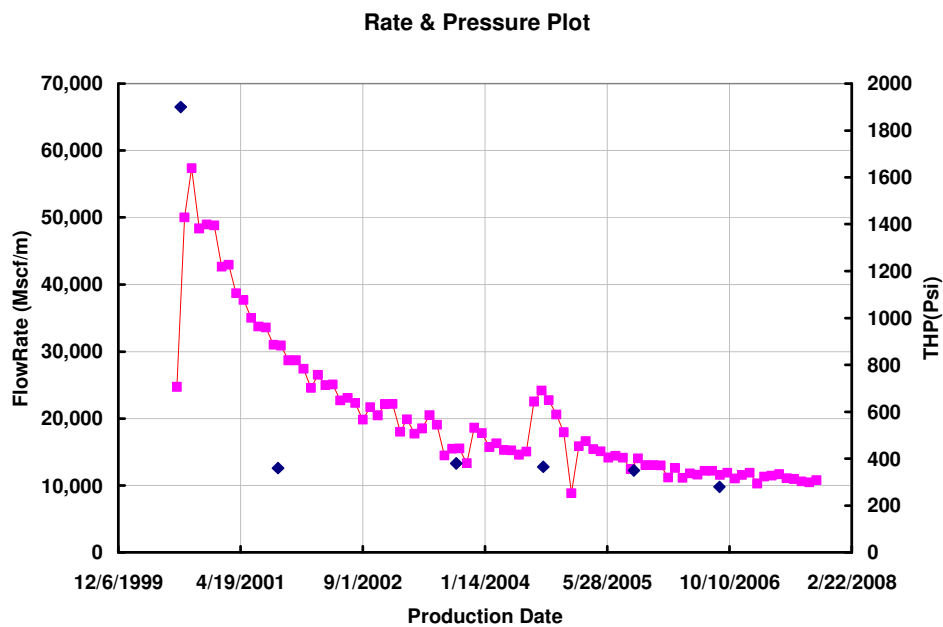
Fig 4-4 Production and Pressure Profile: Well 100000452

4.2   History Match

Productions were analyzed using three different reservoir models: radial homogeneous, power law model, and two wing traditional fractures.

Even though Equivalent Radial Homogeneous models doesn't represent a fractured well it can be used with good approximation for conventional and unconventional formations during pseudo steady state (Jordan, Fenniak, 2006)[12]. In pseudo steady state flow the effective permeability of the ERH model compensates for shape, heterogeneity and damage around the well bore.

Linear flow of two wing fracture (finite or infinite conductivity) model successfully simulates the steep production decline during transient flow. However, declines from Barnett formations well are so steep during transient flow that even linear flow regime sometime fails to simulate this production decline.

This is the first attempt to match the production rate of Barnett formations well with power law model. First step in history matching with this model is to find a correct value for n and R_e. As we have seen power law index could easily be determined by measuring the slope of pressure derivative curve (transient flow) and drainage radius by calculating the time when pseudo steady state flow begins from constant flow rate solutions. Unfortunately constant flow rate pressure data was not available for this analysis. In the absence of it we resorted to constant pressure model which is not as robust as constant rate method but still has the capability to determine a unique value of n and R_e. In this method we directly match the production rate using constant pressure solution. In Section 3.1 this methodology has already been described.

4.2.1 History Match Using Power Law Model

Basic idea in using this model is to find a combination of n, R_e, and k_w for a well through history matching and then to use these parameters for production forecasting. After some initial analysis we found that contrary to the popular belief transient flow in Barnett formation wells are very short spanned. Effect of boundary is seen on production within 2-3 months of flow period. It was also found that a short drainage radius is mainly responsible for steep production decline. In addition, a short drainage radius also hampered the chances of finding unique combination of n & R_e with the analysis of monthly production data. Unique value of n could only be determined by analyzing early stage production when it's not affected by boundary. Having very few data point in this period makes this task difficult. Also the production of fracture fluid and a variable bottom hole pressure during initial flow period makes this task cumbersome and well test data is required to fully validate this model. Nevertheless, after careful analysis we did see the effect of n on production and have proved that a better match to production can be made using this model as it successfully simulate large decline in production rate at early time and a slow decline at late time.

Fig 4-5 to Fig 4-9 shows the results for best matches obtained for various combinations of n and R_e. Solid red circles are the actual production rate and black line is the simulated rate. Solid blue circles are the cumulative production rate and red line is the simulated cumulative rate.

Fig 4-5 represents the closest match for n equal to zero. We obtained this match at n = 0, Re = 350 ft and k_∞ = 0.028 md. However, the simulated production rate at n = 0 is far from a good match. Fig 4-6 is for n equal to 1/2, though the match

is slightly better than n equal to 0 it's again far from being called a good match. Fig 4-7 and Fig 4-8 is for n equal to 1 and 3/2 respectively which is again not a very good match. However, we observe a gradual improvement in match with increased n and the best match is obtained at n = 2, Re = 350 ft and k_∞ = 0.00045 md (Fig 4-9). Results for various n have been tabulated in Table 4-1.

Table 4-1 Results of History Match

Well Name	2540777	2540777	2540777	2540777	2540777
Stimulation Index, n	2	3/2	1	1/2	0
Drainage Radius, R_e (ft)	350	350	350	350	350
Well bore Radius, R_w (ft)	0.328	0.328	0.328	0.328	0.328
Well bore Permeability, K_w (md)	512	38.34	2.454	0.196	0.028
Formation Permeability, K_∞ (md)	0.00045	0.0011	0.0023	0.006	0.028
Thickness, h (ft)	266	266	266	266	266
Initial Pressure, P_i (psi)	3000	3000	3000	3000	3000
Gas Gravity, γ_g	0.7	0.7	0.7	0.7	0.7
Mole fraction, N_2	0	0	0	0	0
Mole fraction, CO_2	0	0	0	0	0
Mole fraction, H_2S	0	0	0	0	0
Porosity, Φ	0.05	0.05	0.05	0.05	0.05
Water Saturation, S_w	0.1	0.1	0.1	0.1	0.1
V_L(scf/ton)	30	30	30	30	30
P_L (psi)	120	120	120	120	120
Spec Gravity Rock, γ_s	2.65	2.65	2.65	2.65	2.65
Initial free gas (mmscf)	741	741	741	741	741
Initial adsorbed gas (mmscf)	272	272	272	272	272
Final Free gas (mmscf)	251	223	213	211	208
Final Adsorbed gas (mmscf)	253	250	248	248	248
Final Pressure (psi)	1024	913	871	862	852
Production time (days)	2650	2650	2650	2650	2650
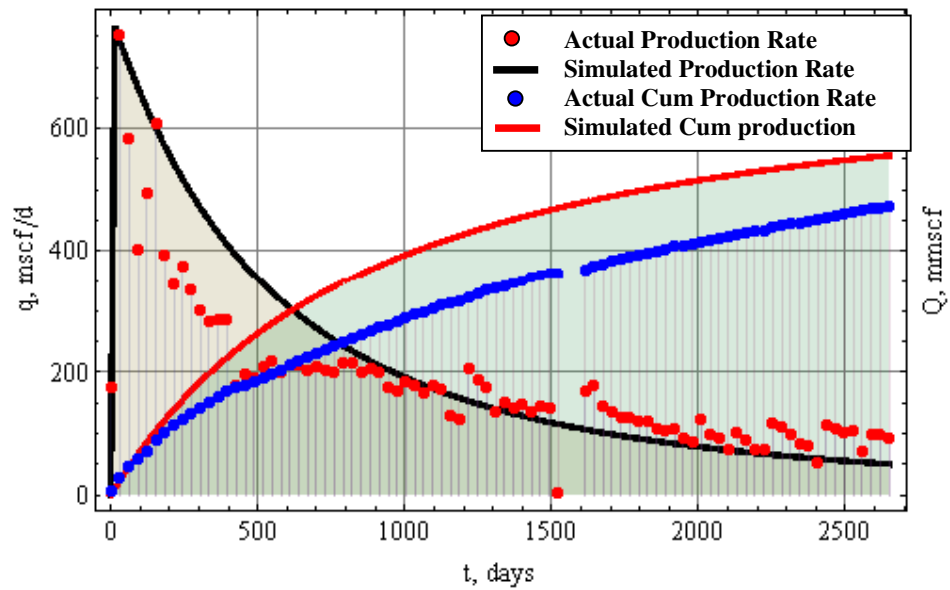
Fig 4-5 Production and Cumulative Production Plot, n = 0
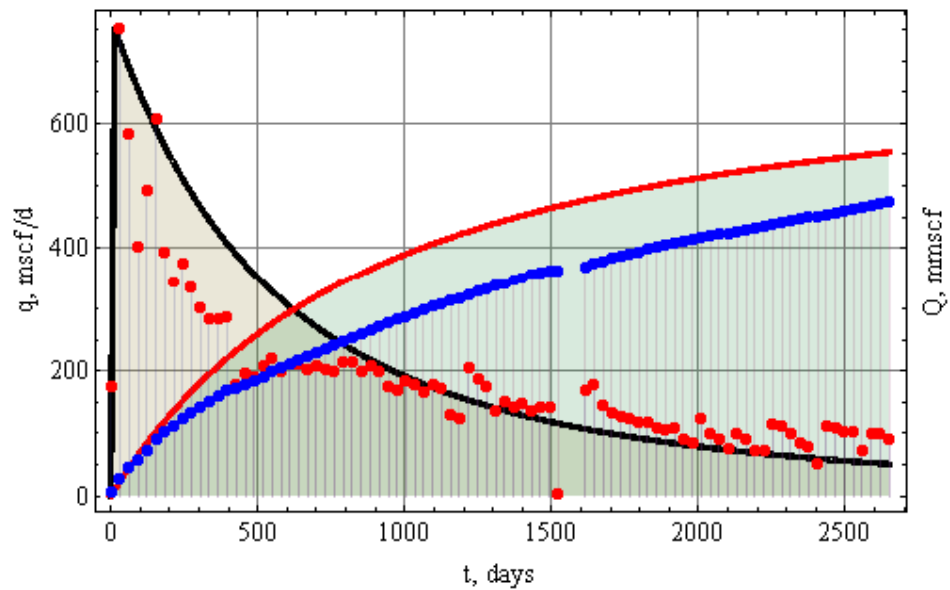
Fig 4-6 Production and Cumulative Production Plot, n = 1/2
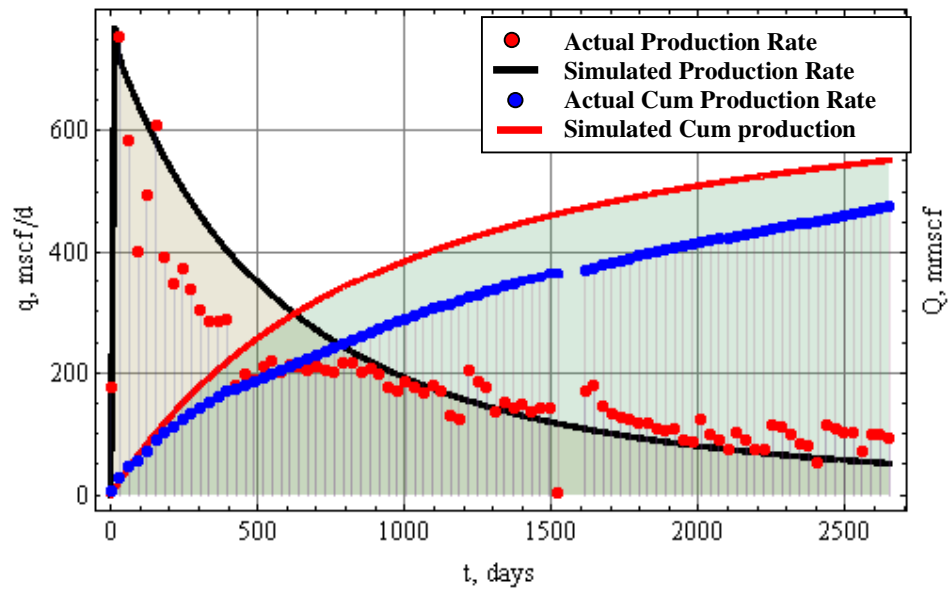
Fig 4-7 Production and Cumulative Production Plot, n = 1
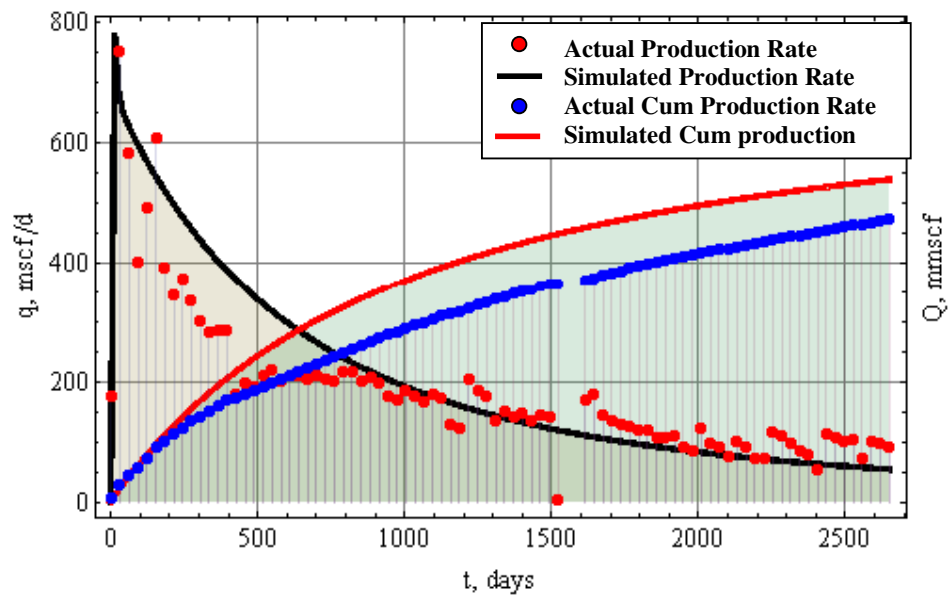
Fig 4-8 Production and Cumulative Production Plot, n = 3/2
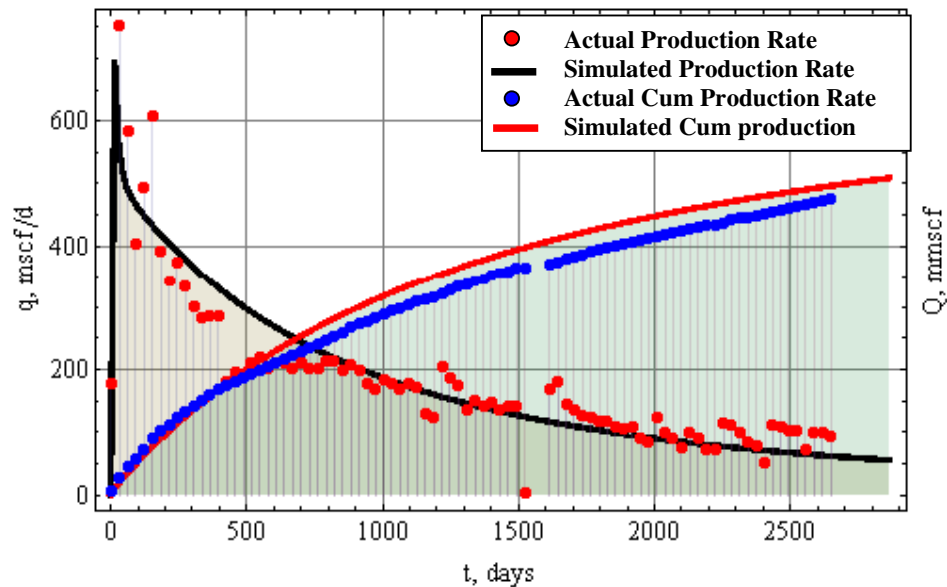
Fig 4-9 Production and Cumulative Production Plot, n = 2

4.2.2 History Match Using Traditional Models

We used well test analysis software Topaze to analyze the radial homogeneous and two wing fracture models. Numerically, these models are different form each other in its use of number of variable parameters. A homogeneous model has just two variables, permeability and drainage radius. Two wing fracture model has three variables: permeability, drainage radius and fracture half length. In dendric model the third variable is power law index.

Fig 4-10 shows the production history match results for two wing fracture model. X-axis represents the time, primary Y-axis indicates the daily production rate, and secondary Y-axis is for cumulative production. Solid red lines are the simulated production rate while the dots are the actual daily and cumulative production rate. Input data and results are summarized in Table 4-2.

We get a poor match for first year production. But once the flow reaches to pseudo-steady state region we observe a good match. Flow geometry becomes irrelevant in pseudo-steady state flow regime. At this time it's not possible to say that two wing fracture geometry is not applicable to Barnett Shale wells. What we have discovered is that two wing fracture model is not the only possibility but its just one of them.

Table 4-2 Results of History Match for Two Wing Model

Well Name	2540777
Fracture Half Length, Xf (ft)	229
Drainage Radius, R_e (ft)	245
Well bore Radius, R_w (ft)	0.328
Average Permeability, K (md)	0.00203
Fracture Conductivity, Fc (md-ft)	0.00045
Thickness, h (ft)	266
Initial Pressure, P_i (psi)	3000
Gas Gravity, γ_g	0.7
Mole fraction, N_2	0
Mole fraction, CO_2	0
Mole fraction, H_2S	0
Porosity, Φ	0.05
Water Saturation, S_w	0.1
V_L(scf/ton)	0
P_L (psi)	0
Initial free gas (mmscf)	911
Initial adsorbed gas (mmscf)	0
Final Free gas (mmscf)	435
Final Adsorbed gas (mmscf)	0
Final Pressure (psi)	1350
Production time (days)	20*365

Standard Model, Material Balance	
Fracture - Finite conductivity	
Homogeneous	
Circle, No flow	
Tmin	0 hr
Tmax	62640 hr
Total Skin	-5.3
k.h, total	0.54 md.ft
k, average	0.00203 md
Pi	3000 psia
STGIIP	0.911 bscf
STGIP	0.435 bscf
Skin	0
Geometrical Skin	-5.3
Xf	229 ft
Fc	1 md.ft
Pi	3000 psia
k.h	0.54 md.ft
k	0.00203 md
Re - No flow	245 ft
TMatch	1.41E-5 [hr]-1
PMatch	6.24E-9 [psi2/cp]-1
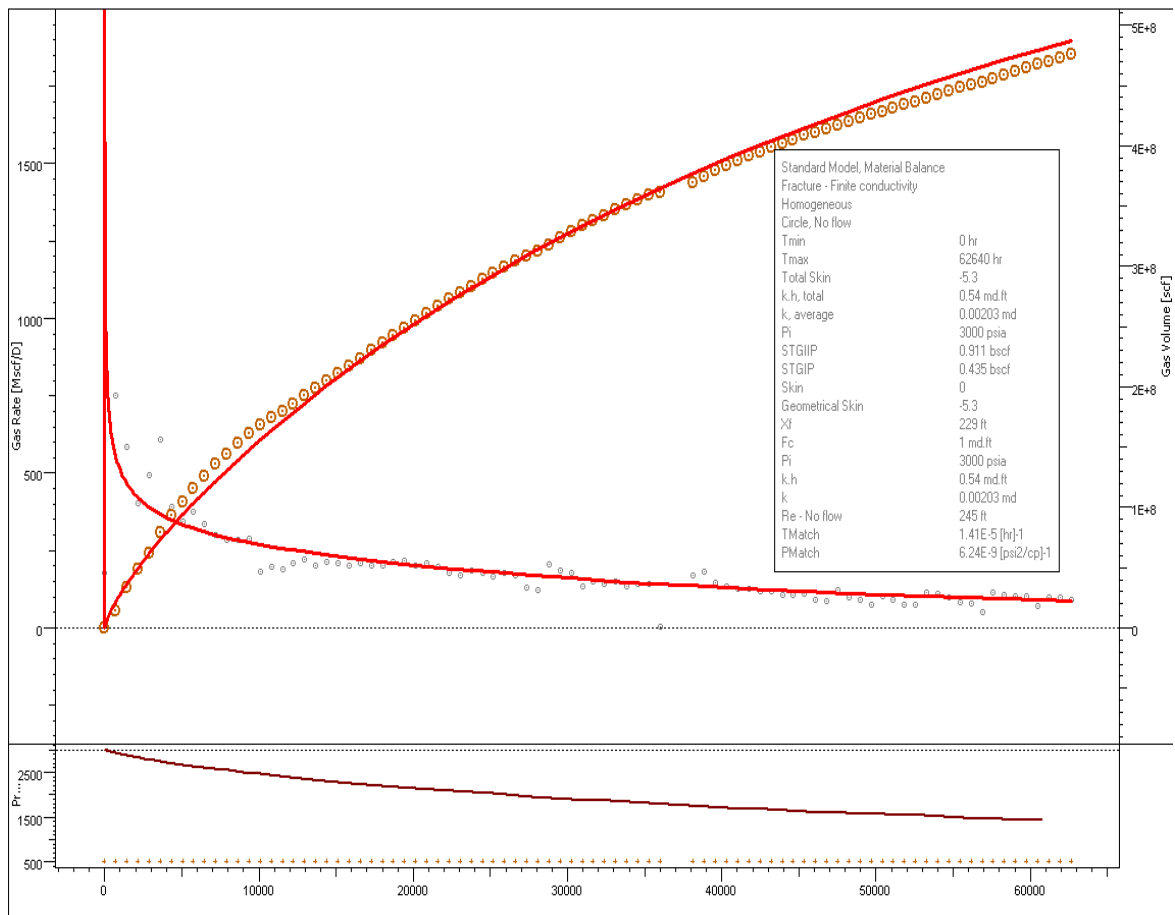
Production history plot (Gas Rate [Mscf/D], Pressure [psia] vs Time [hr])

Fig 4-10 Production and Cumulative Production Plot for Two Wing Fracture Model:
Traditional Model
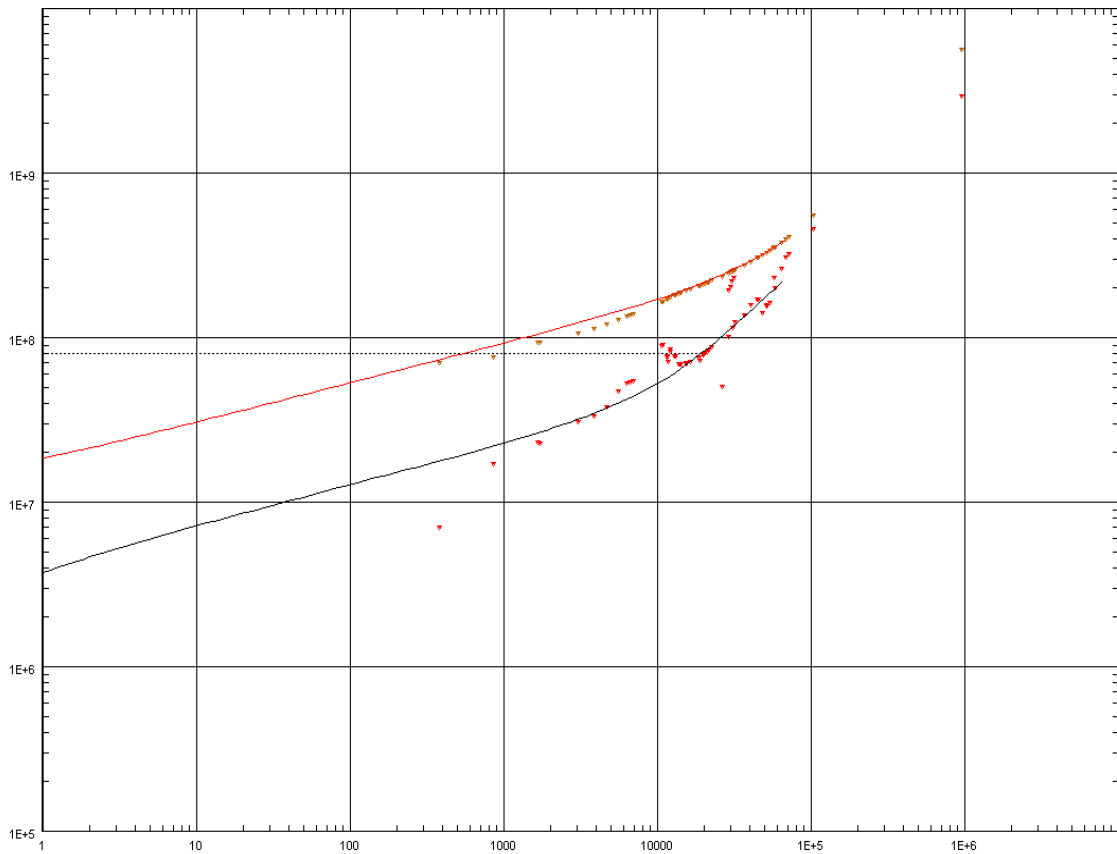
Loglog plot: Normalized pressure Int. and derivative [psi2/cp] vs te [hr]

Fig 4-11 Pressure and Derivative Plot for Two Wing Fracture Model: Traditional Model

Fig 4-11 is Bourdet et al Type curve for two wing models. Normalized pressure integral has been used to reduce the noise in data. Two distinct flow regimes are observed; early time linear flow and late time pseudo-steady state flow. Match is not good in early time.

Fetkovich plot: q [Mscf/D], Q [scf] vs dt [hr]
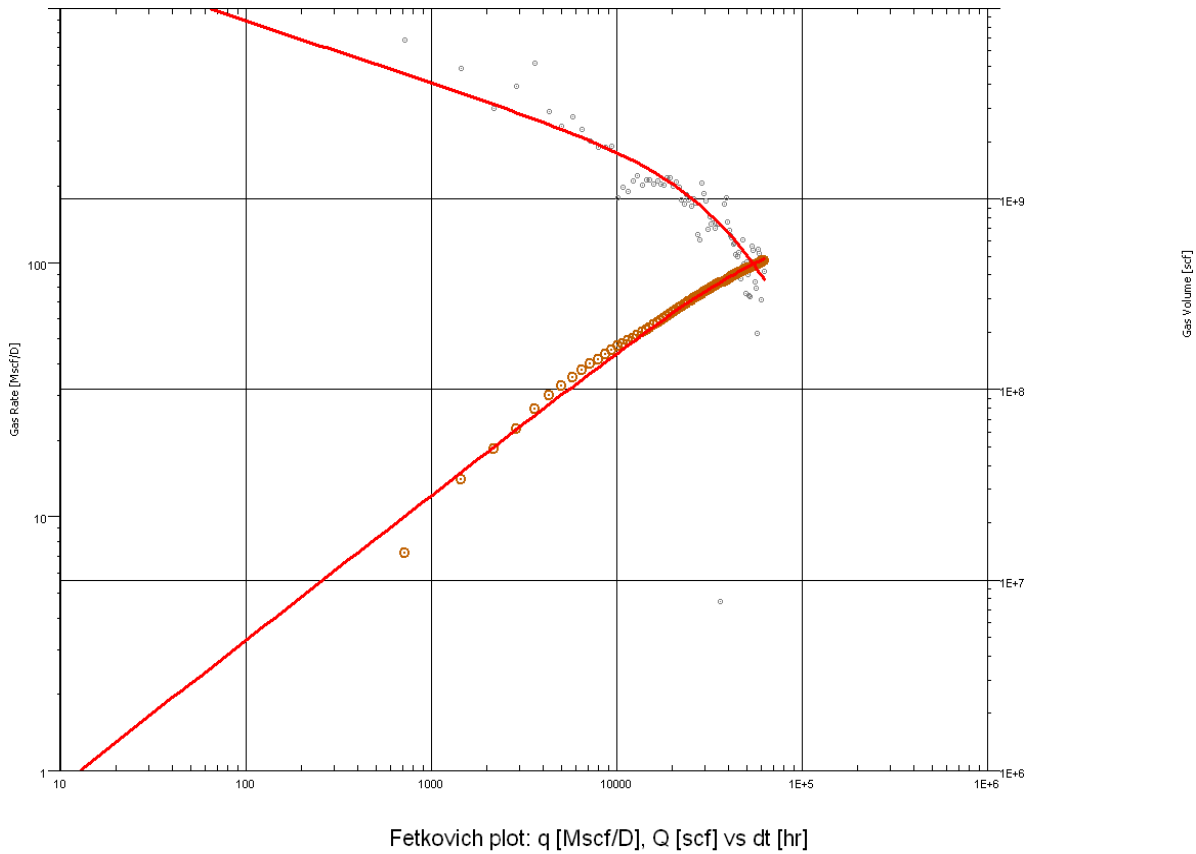
Fig 4-12: Fetkovich Plot for Two Wing Fracture Model: Traditional Model

Fetkovich (SPE 4629) in his work combined the constant pressure solution with the decline curve analysis. Fig 4-12 shows a good match of flow rate with Fetkovich Type curve. Dark dots are actual flow rate and yellow dots are cumulative rate. Red lines are simulated rate with Fetkovich type curve.

Fig 4-13 shows the production history match results from Topaze for radial homogeneous reservoir. X-axis represents the time, primary Y-axis indicates the daily production rate, and secondary Y-axis is for cumulative production rate. Solid red lines are the simulated production rate while the dots are the actual daily and

cumulative production rate. The result is quite similar to what we obtained with dendric model.
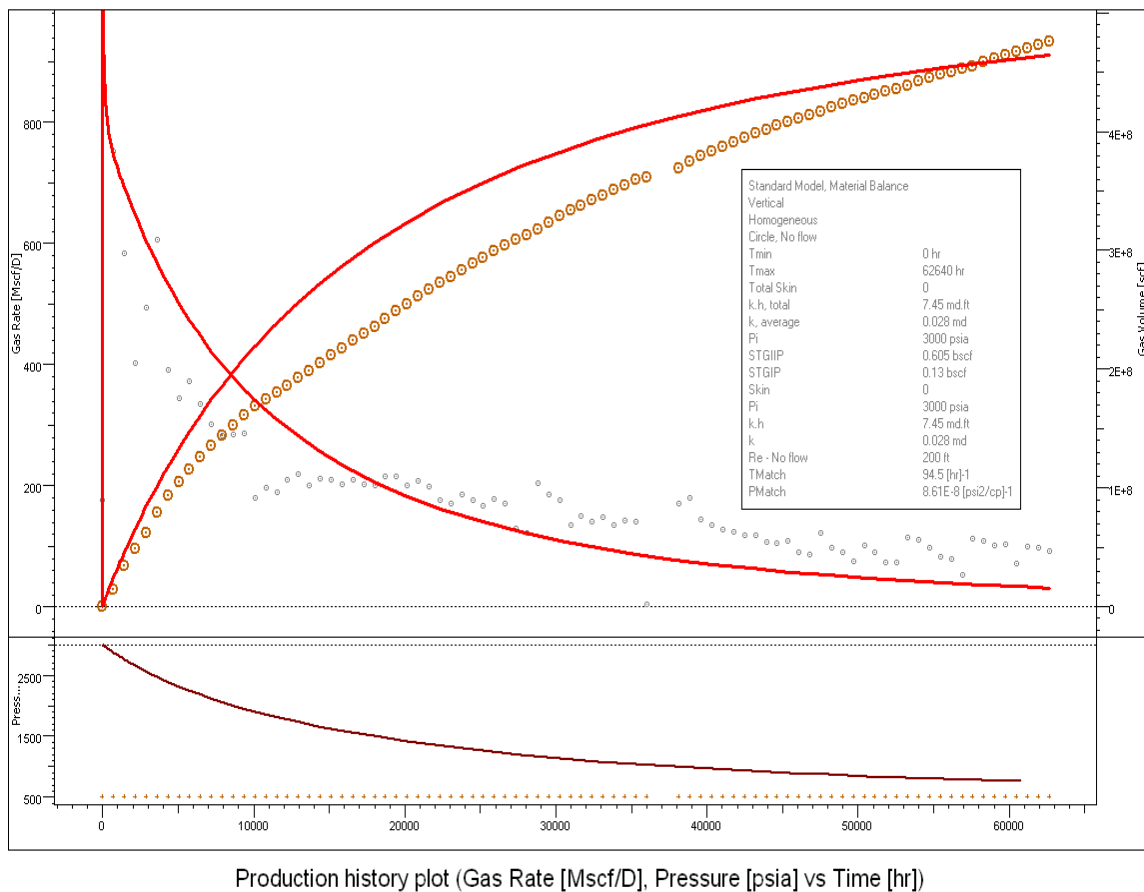
Fig 4-13 Production and Cumulative Production Plot for Radial Homogeneous Case

4.3   Production Forecast

One of the objectives of this research was to investigate the applicability of this model in forecasting the production from Barnett Shale formation wells. After

history matching, a production forecast for any model can be made for anticipated producing pressure.

4.3.1   Well 2540777

Well 2540777 is a vertical well in Barnett formation on production since July 2000. It was stimulated with 1310000 gals of water and 138000 lbs of sand. Initial gas volume in place has been 1.013 bcf; 0.741 bcf in free gas and 0.272 bcf adsorbed gas. Adsorbed gas is around 25% of total gas volume in place which is within the limit of core test result at 20-30%.

A good match is obtained at n and Re values of 2 and 350 ft respectively. On production forecasting we get cumulative production of 0.613 bcf in 20 years from this well that indicates a recovery factor of 60%. Other study in Barnett formation suggests a recovery factor of 15-20 %. It means only 1/3 rd of drainage volume is effectively stimulated. There is a possibility of three times increase in production if we can effectively fracture the whole drainage area. In Table 4-3 the results from this analysis have been given. Fig 4-14 shows the history matching and production forecast for this well.

Table 4-3 Production Forecasting Results for Well 2540777

Well Name	2540777
Stimulation Index, n	2
Drainage Radius, R_e (ft)	350
Well bore Radius, R_w (ft)	0.328
Well bore Permeability, K_w (md)	512
Formation Permeability, K_∞ (md)	0.00045
Thickness, h (ft)	266
Initial Pressure, P_i (psi)	3000
Gas Gravity, γ_g	0.7
Mole fraction, N_2	0
Mole fraction, CO_2	0
Mole fraction, H_2S	0
Porosity, Φ	0.05
Water Saturation, S_w	0.1
V_L(scf/ton)	30
P_L (psi)	120
Spec Gravity Rock, γ_s	2.65
Initial free gas (mmscf)	741
Initial adsorbed gas (mmscf)	272
Final Free gas (mmscf)	161
Final Adsorbed gas (mmscf)	239
Final Pressure (psi)	661
Production time (days)	20*365

A comparison of new model with traditional model is shown in Fig 4-15. The Indigo line shows the results from traditional model. Both models describe the produced history equally well. The difference in forecasted cumulative production after 20 years is less than 5% which is insignificant. Since the wells flow under pseudo steady state for majority of period it makes no difference what model we use for long term forecast.
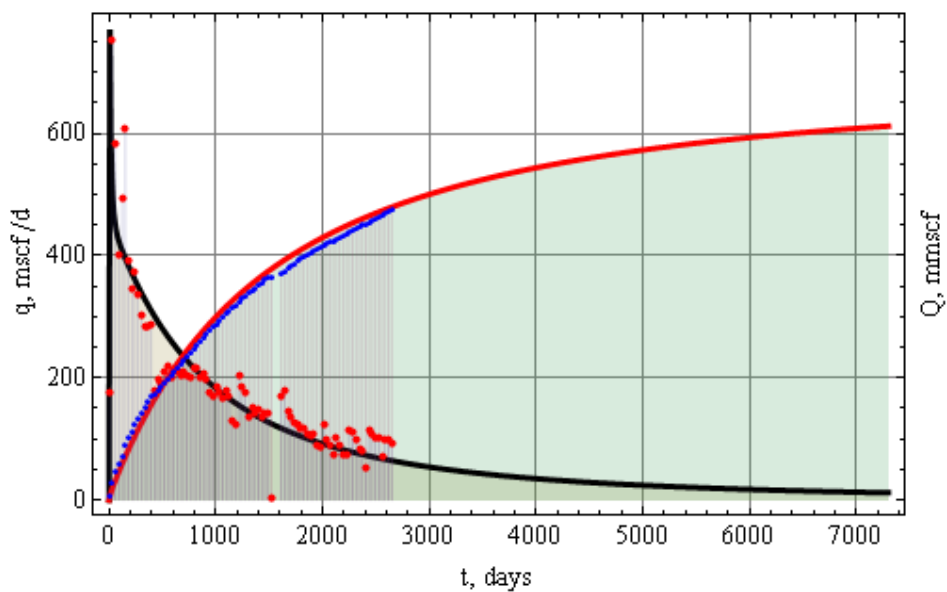
Fig 4-14 Production Forecast by Power Law Model: Well 2540777

Fig 4-15 Comparison of Power law Model with
Traditional Model: Well 2540777

4.3.2   Well 2540767

Well 2540767 is a vertical well in production since June 2000. It was stimulated with 1760000 gals of water and 195150 lbs of sand. Initial gas volume in place has been 1.922 bcf; 1.4 bcf in free gas and 0.516 bcf adsorbed gas. Adsorbed gas is around 27% of total gas volume in place which is within the limit of core test result at 20-30%.

A good match is obtained as the difference in actual and simulated production in 8 years is less than 5%. Values for n and Re are 1 and 375 ft respectively. A low power law index and high stimulated area both indicates a better stimulation success than 2540777. On production forecasting we observe cumulative production of 1.2 bcf in 20 years that means a recovery factor of 60%. It means only 1/3 rd of the drainage volume has been effectively stimulated and there is a possibility of three times increase in production if we can effectively fracture the whole drainage area. In Table 4-4 the results from this analysis has been tabulated. Fig 4-16 shows the history matching and production forecast for this well.

Table 4-4 Production Forecasting Results for Well 2540767

| Well Name	2540767
Stimulation Index, n	1
Drainage Radius, R_e (ft)	375
Well bore Radius, R_w (ft)	0.328
Well bore Permeability, K_w (md)	2.51
Formation Permeability, K_∞ (md)	0.0022
Thickness, h (ft)	440
Initial Pressure, P_i (psi)	3000
Gas Gravity, γ_g	0.7
Mole fraction, N_2	0
Mole fraction, CO_2	0
Mole fraction, H_2S	0
Porosity, Φ	0.05
Water Saturation, S_w	0.1
V_L(scf/ton)	30
P_L (psi)	120
Spec Gravity Rock, γ_s	2.65
Initial free gas (mmscf)	1406
Initial adsorbed gas (mmscf)	516
Final Free gas (mmscf)	274
Final Adsorbed gas (mmscf)	446
Final Pressure (psi)	646
Production time (days)	20*365
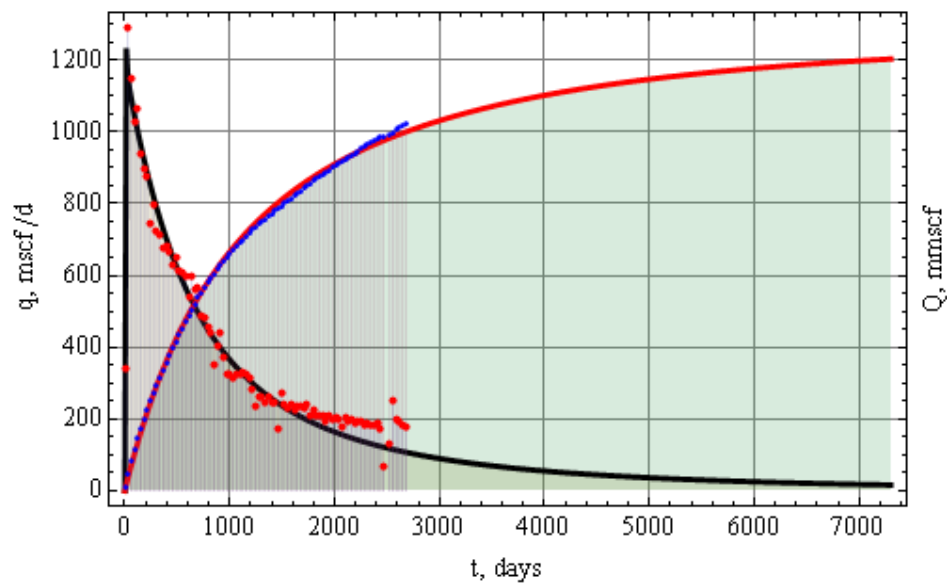
Fig 4-16 Production Forecast by Power Law Model: Well 2540767

A comparison of new model with traditional model for Well 2540767 is shown in Fig 4-17. The Indigo line shows the results from traditional model. Both models describe the produced history equally well. The difference in forecasted cumulative production after 20 years is less than 5% which is again insignificant.
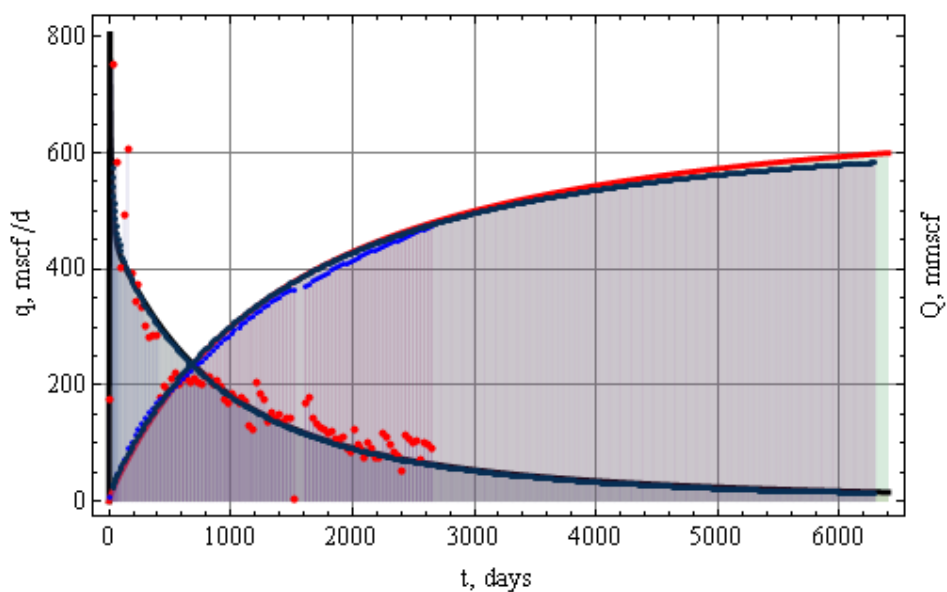

Fig 4-17 Comparison of Power law Model with
Traditional Model: Well 2540767

4.3.3 Well 2540773

Well 2540773 is a vertical well in production since June 2000. It was stimulated with 320000 gals of water and 156000 lbs of sand. Initial gas volume in place has been 1.276 bcf; .934 bcf in free gas and 0.342 bcf adsorbed gas.

A good match is obtained as the difference in actual and simulated production in 8 years is less than 5%. Values for n and Re are 2 and 335 ft respectively. On production forecasting we get cumulative production of 0.773 bcf in 20 years that suggests a recovery factor of 60%. It means only 1/3 rd of the drainage

volume has been effectively stimulated and there is a possibility of three times increase in production. Results from this analysis have been given in Table 4-5. Fig 4-18 shows the history matching and production forecast for this well.

Table 4-5 Production Forecasting Results for Well 2540773

| Well Name	2540773
Stimulation Index, n	2
Drainage Radius, R_e (ft)	335
Well bore Radius, R_w (ft)	0.328
Well bore Permeability, K_w (md)	478
Formation Permeability, K_∞ (md)	0.00042
Thickness, h (ft)	366
Initial Pressure, P_i (psi)	3000
Gas Gravity, γ_g	0.7
Mole fraction, N_2	0
Mole fraction, CO_2	0
Mole fraction, H_2S	0
Porosity, Φ	0.05
Water Saturation, S_w	0.1
V_L(scf/ton)	30
P_L (psi)	120
Spec Gravity Rock, γ_s	2.65
Initial free gas (mmscf)	934
Initial adsorbed gas (mmscf)	342
Final Free gas (mmscf)	202
Final Adsorbed gas (mmscf)	301
Final Pressure (psi)	682
Production time (days)	20*365
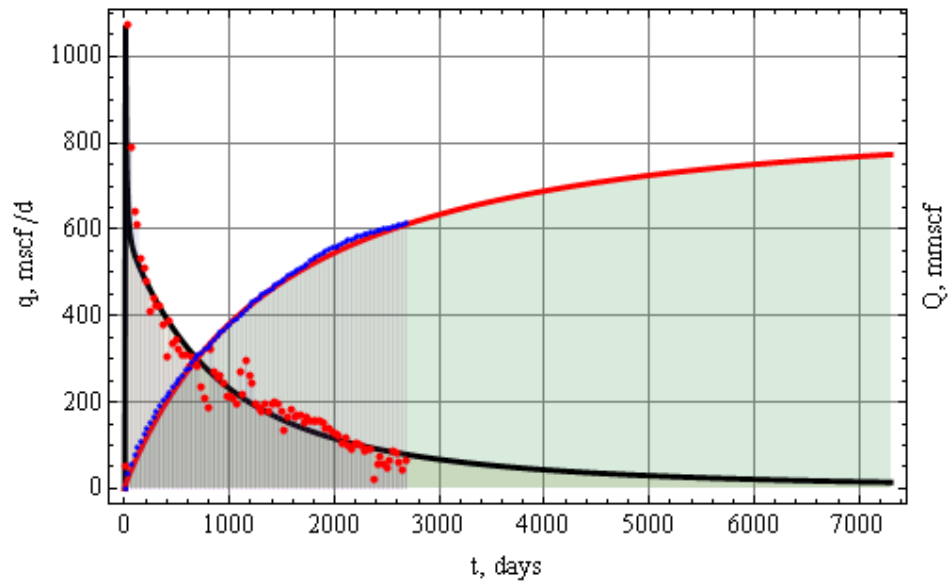
Fig 4-18 Production Forecast by Power Law Model: Well 2540773

A comparison of new model with traditional model is shown in Fig 4-19. The Indigo line shows the results from traditional model. Both models describe the produced history equally well. Similar to the previous results there is not much difference in forecasted production over twenty years period.
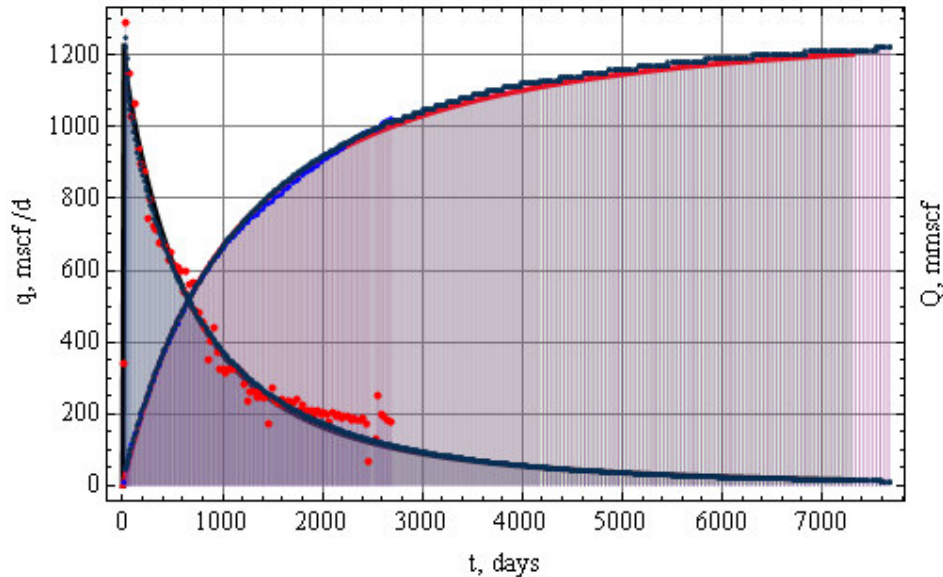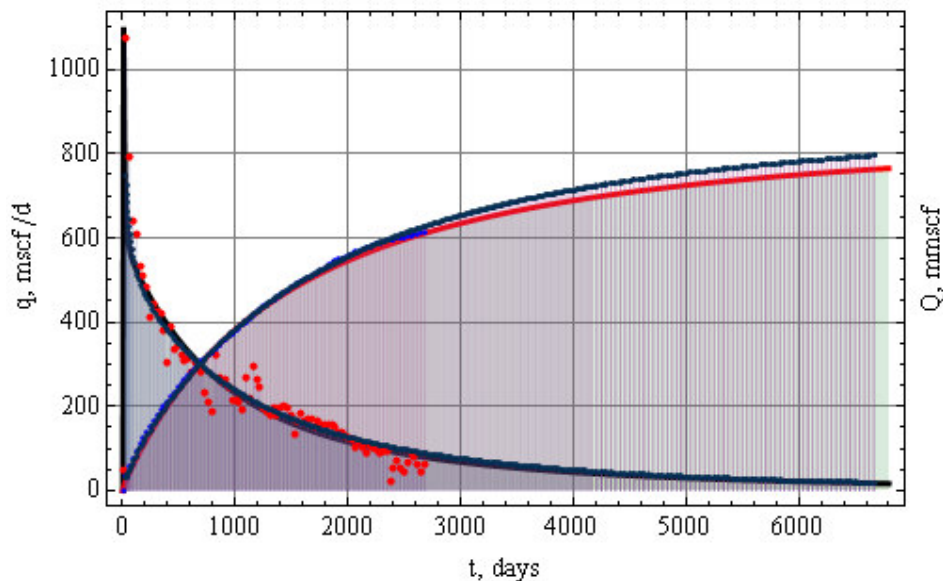
Fig 4-19 Comparison of Power Law Model with
Traditional Model: Well 2540773

4.3.4   Well 100000452

Well 100000452 is a vertical well in production since August 2000. It was stimulated with 1420000 gals of water and 178000 lbs of sand. This well was re-stimulated in August 2004. Initial gas volume in place has been 3.657 bcf; 2.676 bcf in free gas and 0.981 bcf adsorbed gas.

A good match was observed before the re-stimulation Fig 4-20. Results from this analysis have been given in Table 4-6. Re-stimulation exposes more formation rock to production that increases the production rate. This model will under predict the production rate and total recovery for a re-stimulated well.

Table 4-6 Production Forecasting Results for Well 100000452

| Well Name	100000452
Stimulation Index, n	1
Drainage Radius, R_e (ft)	600
Well bore Radius, R_w (ft)	0.328
Well bore Permeability, K_w (md)	7.317
Formation Permeability, K_∞ (md)	0.004
Thickness, h (ft)	327
Initial Pressure, P_i (psi)	3000
Gas Gravity, γ_g	0.7
Mole fraction, N_2	0
Mole fraction, CO_2	0
Mole fraction, H_2S	0
Porosity, Φ	0.05
Water Saturation, S_w	0.1
V_L(scf/ton)	30
P_L (psi)	120
Spec Gravity Rock, γ_s	2.65
Initial free gas (mmscf)	2676
Initial adsorbed gas (mmscf)	981
Final Free gas (mmscf)	596
Final Adsorbed gas (mmscf)	867
Final Pressure (psi)	676
Production time (days)	20*365
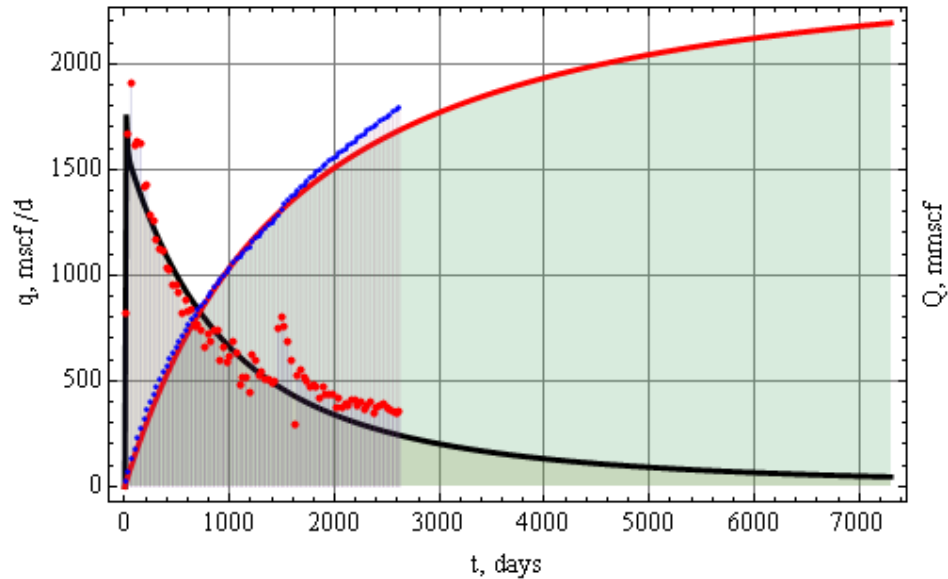
Fig 4-20 Production Forecast by Power Law Model: Well 100000452

A comparison of new model with traditional model is shown in Fig 4-21. The Indigo line shows the results from traditional model. This well is a re-stimulation candidate. None of the model provides a good productivity behavior after re-stimulation.
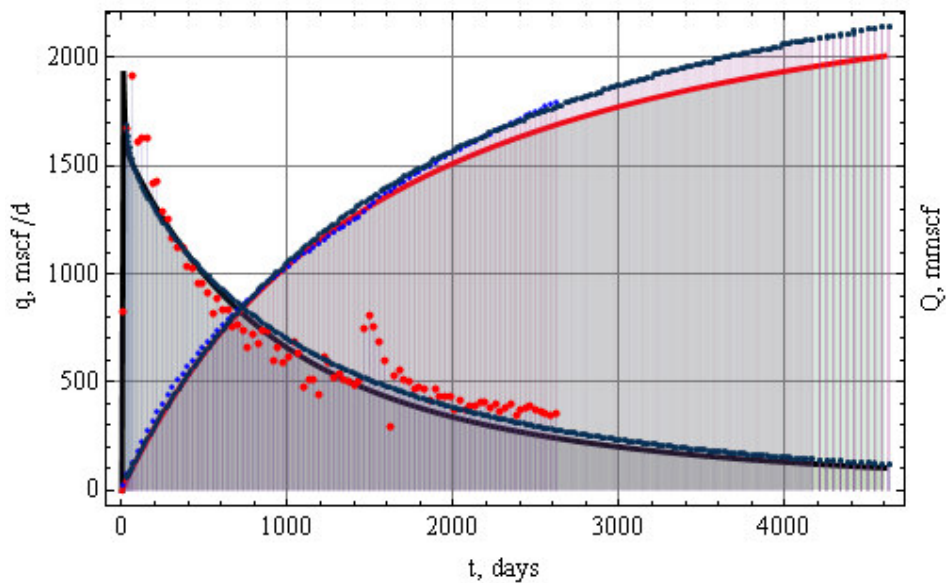
Fig 4-21 Comparison of Power law Model with
Traditional Model Well 100000452

Summary of production forecasting result for all the above cases is given in

Table 4-7.

Table 4-7 Summary of Production Forecasting Result

Well Name	n	Thickness (ft)	Drainage Radius (ft)	Stimulated Rock Volume (mmcf)	Wellbore Perm (md)	OGIP (mmscf)	Cum Prod (PL Model) (mmscf)	Cum Prod (Trad Model) (mmscf)
2540777	2	266	350	102	512	1013	613	641
2540767	1	440	375	194	0.62	1922	1202	1212
2540773	2	366	335	129	478	1276	773	806
100000452	1	327	600	370	7.32	3657	2184	2354

A very good correlation is obtained between effective stimulated rock volume

and EUR (Fig 4-22). It is based on the study of ten different wells. The database

includes the wells drilled in 80's as well as the wells producing for last 3 years. EUR

was calculated using Power Law as well as traditional model and average of two was taken.
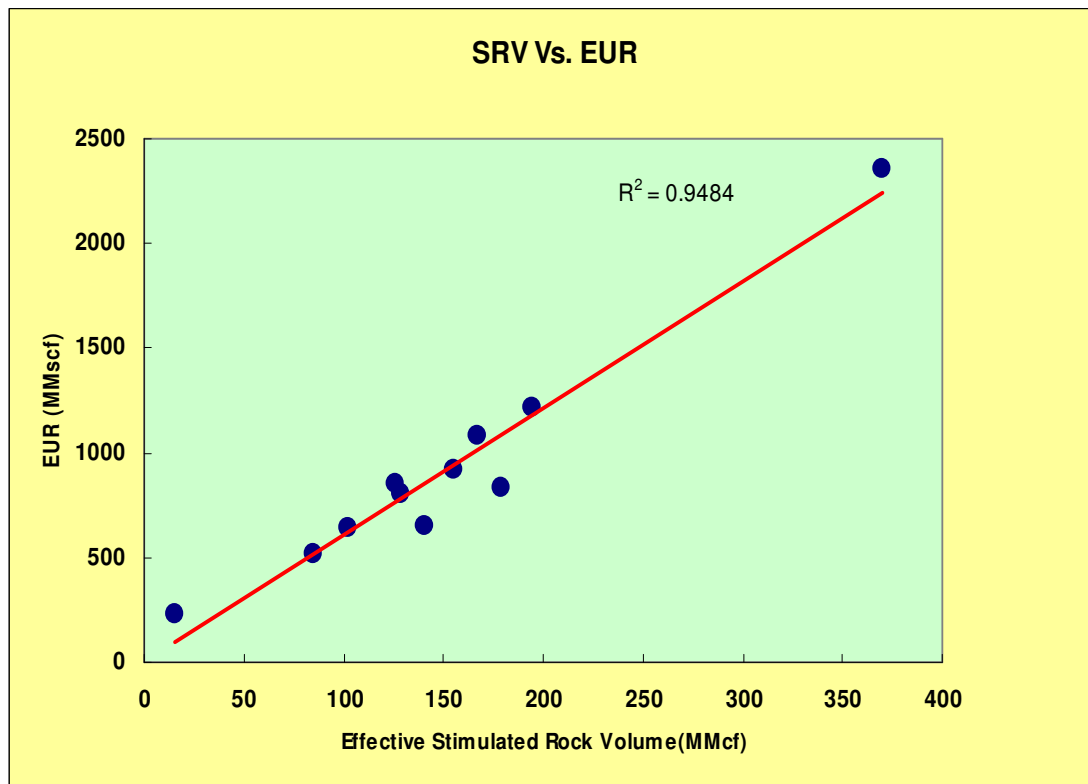
Fig 4-22 Effect of SRV on EUR

4.4   Discussion

Barnett Shale formation wells flow under pseudo steady state for most part of its producing life. The flow is highly dominated by the boundary. In this case boundary refers to the area effectively stimulated by fracture treatment. Whatever the little effect permeability distribution has on production is limited to initial few months when the flow is still under transient state. Reservoir permeability can be

described by a single valued average permeability during PSS flow and its distribution has no effect on production during this period.

Due to a short period of transient flow production from Barnett formation is expected to be largely independent of the relative distribution of permeability and highly dependent on the stimulated area and created secondary permeability. However, an indirect relationship between permeability distribution and production rate is observed. It could better be understand with power law index value. A well with low power law index shows a better (more even) secondary permeability distribution, larger stimulated volume and better production. This correlation becomes intuitive when we analyze sand placement in the formation. On placing large volume of sand around well bore we place less volume away from the wells and thus create a steeply declined permeability indicated by high power law index. It also results in low stimulated volume and low average permeability as less sand was placed away from the well bore. Similarly when we are able to place the sand evenly in the formation we get larger stimulated volume and average permeability indicated by low value of power law index.

EUR of the wells is a direct function of effective stimulated rock volume. This is the single most dominant parameters that determine the ultimate recovery of wells.

At 25-30% adsorbed gas volume, we dint observe significant contribution of adsorbed gas in production from Barnett shale formation. It also explains why we don't see any difference in forecasted production with new model that accounts for adsorbed gas production and traditional mode that doesn't include adsorbed gas production. However, new experimental results suggest adsorbed gas in Barnett shale

could be around 40-60 %. At this percentage level, forecasted production with two models will be significantly different. The results form new model will be more reliable.

There are some limitations of this model. This model is limited to constant rate and constant pressure flow only. It is applicable for single phase fluid. This model can't be used for production forecasting unless production history of at least one year is available.

In this work we didn't have the micro seismic maps of the wells so couldn't determine the correlation between effective stimulated and acoustic volume.

5   SUMMARY AND CONCLUSIONS

5.1   Summary

The primary objective of this work was to check the applicability of Power Law permeability model for Barnett Formation wells. Type curves for constant flow rate case were generated to determine the two important formation properties; drainage radius and power law index. Furthermore pressure solution was combined with material balance to make production forecast for constant pressure flow. History matching was performed and production forecast was made for 20 years of production.

EUR of a well is found to be a direct function of the gas volume in place connected to the well bore after stimulation treatment. The volume of gas that connects to the wellbore depends on the extent and density of fracture networks.

A good indicator of successful fracture stimulation is power law index. A low power law index indicates high density of fracture network and better production. Good producers have low power law index and large drainage radius. One with high density of fracture network indicates more even distribution of permeability while one with less fracture network density suggests larger permeability at well bore and a low permeability away from the well bore. A distinct difference in the distribution of permeability observed for low and high producing wells. From this analysis it can also be concluded that pumping sand is essential to create secondary permeability in the Barnett Shale formation.

The following conclusions were made from this work:

a) A power law permeability model can be used to describe the effect of large water to sand ratio stimulation treatments in the Barnett Shale.

b) Case studies show that only 1/3rd of the drainage volume calculated from well spacing is effectively stimulated.

c) Cumulative production is mainly determined by the total gas in place connected to the well bore through the fracture network.

d) Lower power law index obtained from history match indicates more evenly stimulated drainage volume and higher sustained production rates.

e) Variable well bore pressure during initial production makes it difficult to determine the accurate value of the power law index. Well test data would be necessary to accurately determine the power law index.

f) Because of uncertainty in the estimated power law index, the most influential parameter seems to be the drainage radius.

REFERENCES

1. Hill, D. G., and C. R. Nelson,: "Gas productive fractured Shales—an overview and update", *GasTIPS*, 2000,Vol. 6 No. 2. 4-13.

2. Kuuskraa, A. Vello: "Unconventional Gas-1", *Oil & Gas Journal*, Sept. 3, 2007, Vol. 35.

3. Fisher, M.K.,Wright C.A., Davidson, B.M., Goodwin, A.K.,Fielder, E.O.,Buckler, W.S. and Steinsberger, N.P., "Integrated Fracture Mapping Technologies to Optimize Stimulations in the Barnett Shale," paper SPE 77441 presented at the SPE Annual Technical Conference and Exhibition , San Antonio, Texas, 29 September- 2 October 2002.

4. Valkó, P. P. and Mursal, Fnu: "New Approach for Interpreting Pressure Transient Test After Massive Acidizing Treatment," paper SPE 77623 presented at the SPE Annual Technical Conference and Exhibition, San Antonio, Texas, 29 September–2 October 2002.

5. Weng, Xiaowei, Siebrits, Eduard, 2008 , "Simulations for Hydraulic Fracturing Treatments and Methods of Fracturing Naturally Fractured Formation," United States, Patent Number 20080183451, http://www.freepatentsonline.com/ 2008 0183451. html

6. Abate, J. and Valkó, P.P.: "Multi-precision Laplace transform inversion," *International Journal for Numerical Methods in Engineering,* 2004, Vol. 60, Issue 5-7.

7. MATHEMATICA, Version Number 6.0.1.0, Wolfram Research Inc.,United States, Inc.100 Trade Center Drive Champaign , IL 61820-7237, (2007).

8. Bourdet, D. et al.: "A New Set of Type Curves Simplifies Well Test Analysis," *World Oil*, May 1983, 95-106.

9. Helmy, M. W. and Wattenbarger, R. A. : "Productivity of Wells Producing at Constant Pressure," paper SPE 39970 presented at the 14 th EGPC Conference, Cairo, Egypt, October 12-15, 1998.

10. Helmy, M. W. and Wattenbarger, Robert A.: "New Shape Factors for Wells Producing at Constant Pressure," *In-Situ*, Volume 23, Issue No. 2, May 1999.

11. Ecrin v 4.10, Topaze v 4.10, Kappa Solutions, 2008.

12. . Jordan, C.L., Fenniak, M.J., Smith, C.R., Rapid Technology Corp., "Case Studies: A Practical Approach to Gas-Production Analysis and Forecasting," Paper 99351, SPE Gas Technology Symposium, Calgary, Alberta, Canada,15-17 May, 2006.

APPENDIX A

DEVELOPMENT OF THE SOLUTION

Development of the Model

Following well known diffusivity equation in dimensionless form is used

$$\frac{1}{r}\partial_r(k_r r \partial_r p) = \phi \mu c_t \partial_t p \qquad \textbf{where} \qquad k_r = k_w \left(\frac{r_w}{r}\right)^n$$

Initial and Boundary Conditions

$$p(r,0) = p_i \qquad \qquad \textbf{(Initial Condition)}$$

$$rk_r \frac{\partial p}{\partial r}\bigg|_{r=r_w} = \frac{qB\mu}{2\pi h} \qquad \textbf{(Constant Rate Inner Boundary)}$$

$$p\big|_{r=r_e} = p_i \qquad \textbf{(Constant Pressure Outer Boundary)}$$

$$\frac{\partial p}{\partial r}\bigg|_{r=r_e} = 0 \qquad \textbf{(No Flow Outer Boundary)}$$

To convert the equation in standard form we define some dimensionless variable as:

$$p_D = \frac{2\pi k_w h}{qB\mu}(p_i - p)$$

$$t_D = \frac{k_w}{\phi \mu c_t r_w^2} t$$

$$r_D = \frac{r}{r_w}$$

$$k_D = \frac{k_r}{k_w}$$

Introducing the dimensionless variables

$$\frac{1}{r_D}\frac{\partial}{\partial r_D}(k_D r_D \frac{\partial p_D}{\partial r_D}) = \frac{\partial p_D}{\partial t_D} \quad \textbf{Where} \quad k_D = \left(\frac{1}{r_D}\right)^n$$

Initial and Boundary Conditions

$$p_D(r,0) = 0 \qquad\qquad \textbf{(Initial Condition)}$$

$$r_D k_D \left.\frac{\partial p_D}{\partial r_D}\right|_{r_D=1} = -1 \qquad \textbf{(Constant Rate Inner Boundary)}$$

$$p_D\big|_{r=r_{De}} = 0 \qquad\qquad \textbf{(Constant Pressure Outer Boundary)}$$

$$\left.\frac{\partial p_D}{\partial r_D}\right|_{r=r_{De}} = 0 \qquad\qquad \textbf{(No Flow Outer Boundary)}$$

A transformation is used to simplify the equation in order to get a universal solution in terms of stimulation power index n. The new equation and boundary condition with transformed parameter is given below.

Transformation:

$$r = Exp(x)$$

$$x = Log(r)$$

$$x_w = Log(r_w)$$

$$x_e = Log(r_e)$$

$$x_D = x - x_w = Log(r_D)$$

$$x_{De} = x_e - x_w = Log(r_{De})$$

$$k_x = k_w e^{-n(x-x_w)}$$

$$k_{x_D} = \frac{k_x}{k_w} = e^{-nx_D}$$

Let

$$p(e^{x_D}, t_D) = p_{x_D}$$

The diffusivity equation after using transformation

$$e^{-2x_D} \partial_{x_D}(k_{x_D} \partial_{x_D} p_{x_D}) = \varphi \mu c_t \partial_{t_D} p_{x_D}$$

Initial and Boundary Conditions

$$p_{x_D}\big|_{t=0} = 0 \qquad\qquad \textbf{(Initial Condition)}$$

$$k_{x_D} \frac{\partial p_{x_D}}{\partial x_D}\bigg|_{x_D=0} = \frac{qB\mu}{2\pi h} \qquad\qquad \textbf{(Constant Rate Inner Boundary)}$$

$$p_{x_D}\big|_{x=x_{De}} = 0 \qquad\qquad \textbf{(Constant Pressure Outer Boundary)}$$

$$\frac{\partial p_{x_D}}{\partial_{x_D}}\bigg|_{x=x_{De}} = 0 \qquad\qquad \textbf{(No Flow Outer Boundary)}$$

APPENDIX B

COMPOSITE RADIAL MODEL

Inner region equation:

$$\frac{1}{r}\frac{\partial}{\partial r}\left(k_r\, r\,\frac{\partial p_1}{\partial r}\right) = \phi\mu\, c_t\,\frac{\partial p_1}{\partial t} \qquad\qquad r_s < r < r_e$$

$$\frac{1}{r}\frac{\partial}{\partial r}\left(r\,\frac{\partial p_2}{\partial r}\right) = \frac{\phi\mu\, c_t}{k_f}\,\frac{\partial p_2}{\partial t} \qquad\qquad r < r_s$$

$$p_1(r,0) = p_2(r,0) = p_i \qquad\qquad \textbf{(Initial Condition)}$$

$$rk_r\left.\frac{\partial p_1}{\partial r}\right|_{r=r_s} = rk\left.\frac{\partial p_2}{\partial r}\right|_{r=r_s} \qquad\qquad \textbf{(Intermediate Boundary Condition)}$$

$$rk_r\left.\frac{\partial p_1}{\partial r}\right|_{r=r_w} = \frac{qB\mu}{2\pi h} \qquad\qquad \textbf{(Constant Rate Inner Boundary)}$$

$$\left.\frac{\partial p_2}{\partial r}\right|_{r=r_e} = 0 \qquad\qquad \textbf{(No Flow Outer Boundary)}$$

$$\left. p_1\right|_{r=r_s} = \left. p_2\right|_{r=r_s} \qquad\qquad \textbf{(Intermediate Boundary Condition)}$$

APPENDIX C

DIMENSIONLESS PRODUCTIVITY INDEX FOR CONSTANT RATE

In production engineering, the productivity index is defined as the ability of the

reservoir to produce hydrocarbon per unit pressure drop in the reservoir

(volume/time/pressure).

$$J = \frac{q}{(p_{ave} - p_{wf})}$$ .... (C1)

Where q = Flow Rate, p_{ave} = Average Reservoir Pressure, p_{wf} = Well Flowing

Pressure

Introducing the Dimensionless parameters as the followings the expression for the

Dimensionless productivity index would be obtained.

$$p_{D,trad} = \frac{2\pi kh}{qB\mu}(p_i - p)$$ .... (C2)

$$J_D = \frac{\mu B}{2\pi kh} J$$ .... (C3)

Where: P_i = Initial Reservoir Pressure, k = Reservoir Permeability, h = Reservoir

Thickness

B = Formation Volume Factor, μ = Fluid Viscosity

Combining Eqs. 1 through 3 we have:

$$J_D = \frac{1}{p_{D,trad} - p_{D,ave,trad}}$$ .... (C4)

Assuming a constant compressibility during depletion we can write:

$$c_t = -\frac{1}{V}\frac{\partial p}{\partial V}$$ .... (C5)

$$V = \phi Ah$$ .... (C6)

$$\frac{\partial p}{\partial V} = \frac{1}{\phi A h c_t} = cte \quad \dots\dots\dots\dots\dots\dots\dots\dots\dots\dots\dots\dots\dots\dots\dots\dots\dots\dots\dots \text{(C7)}$$

$$\Delta p = p_{ave} - p_i = \frac{\Delta V}{\phi A h c_t} = \frac{N_p B}{\phi A h c_t} = \frac{qBt}{\phi A h c_t} \quad \text{(Constant flow rate production)} \dots\dots\dots \text{(C8)}$$

Using the definition for dimensionless pressure and applying it on Eq. B.8 we

have:

$$p_{D,ave,trad} = \frac{2\pi kh}{qB\mu}(P_i - P_{avg}) = 2\pi \frac{kt}{\phi\mu c_t A} = 2\pi t_{DA} \quad \dots\dots\dots\dots\dots\dots\dots\dots\dots \text{(C9)}$$

Where

$$t_{DA} = \frac{kt}{\phi\mu c_t A} \quad \text{(Dimensionless time defined based on drainage area)} \dots\dots\dots\dots \text{(C10)}$$

Combination of Eqs. C9 and C4 would lead us to an expression correlating the

dimensionless productivity index as a function of dimensionless pressure and

dimensionless time. (Eq. C11)

$$J_D = \frac{1}{p_{D,trad} - 2\pi t_{DA}} \quad \dots\dots\dots\dots\dots\dots\dots\dots\dots\dots\dots\dots\dots\dots\dots\dots\dots \text{(C11)}$$

APPENDIX D

DIMENSIONLESS PRODUCTIVITY INDEX FOR CONSTANT PRESSURE

Dimensionless productivity index for constant pressure solution is given by
(Wattenberger):

$$J_D = \frac{1}{\dfrac{1}{q_D}\left(1 - \dfrac{2Q_D}{r_{De}^2}\right)} \quad \text{.. (D1)}$$

In production engineering, the productivity index is defined as the ability of the

reservoir to produce hydrocarbon per unit pressure drop in the reservoir

(volume/time/pressure).

$$J = \frac{q}{(p_{ave} - p_{wf})} \quad \text{.. (D2)}$$

Where q = Flow Rate, p_{ave} = Average Reservoir Pressure, p_{wf} = Well Flowing

Pressure

Introducing the Dimensionless parameters as the followings the expression for the

Dimensionless productivity index would be obtained.

$$p_{D,trad} = \frac{2\pi kh}{qB\mu}(p_i - p) \quad \text{... (D3)}$$

$$J_D = \frac{\mu B}{2\pi kh}J \quad \text{.. (D4)}$$

Where: P_i = Initial Reservoir Pressure, k = Reservoir Permeability, h = Reservoir

Thickness

B = Formation Volume Factor, μ = Fluid Viscosity

Combining Eqs. D2 through D4 we have:

$$J_D = \frac{1}{p_{D,trad} - p_{D,ave,trad}} \quad \text{..} \quad \text{(D5)}$$

Assuming a constant compressibility during depletion we can write:

$$c_t = -\frac{1}{V}\frac{\partial p}{\partial V} \quad \text{...} \quad \text{(D6)}$$

$$V = \phi A h \quad \text{...} \quad \text{(D7)}$$

$$\frac{\partial p}{\partial V} = \frac{1}{\phi A h c_t} = cte \quad \text{...} \quad \text{(D8)}$$

$$\Delta p = p_{ave} - p_i = \frac{\Delta V}{\phi A h c_t} = \frac{N_p B}{\phi A h c_t} \quad \text{...} \quad \text{(D9)}$$

Using the definition of dimensionless cumulative volume:

$$Q_D = \frac{2 N_p B}{\phi c_t r_w^{\,2} h (P_i - P_{wf})} \quad \text{..} \quad \text{(D10)}$$

Solving equation (D9) & (D10)

$$\Delta p = p_{ave} - p_i = \frac{\Delta V}{\phi A h c_t} = \frac{2 Q_D \phi c_t r_w^{\,2} h (P_i - P_{wf})}{\phi A h c_t} \quad \text{................................} \quad \text{(D11)}$$

Also,

$$p_{D,ave,trad} = \frac{2\pi k h}{q B \mu}(P_i - P_{avg}) = \frac{2\pi k h Q_D}{r_{De}^{\,2} q B \mu}(P_i - P_{wf}) \quad \text{...................................} \quad \text{(D12)}$$

Substituting equation (D12) in equation (D5) we get,

$$J_D = \frac{q_D}{1 - \dfrac{2 Q_D}{r_{De}^{\,2}}} \quad \text{...} \quad \text{(D13)}$$

APPENDIX E

NATURAL GAS CORRELATIONS

Conversion of gas pseudo pressure into real pressure requires many gas properties to be calculated as a function of pressure at a given temperature. These gas properties are explained here. Standard correlations were used to generate the plots.

Fig E1 shows Compressibility Factor vs. Pressure. This is the measure of deviation from ideal gas. We have used computer solution of Standing & Katz (1942) chart for z-factor that was originally developed by Beggs and Brill (1974).
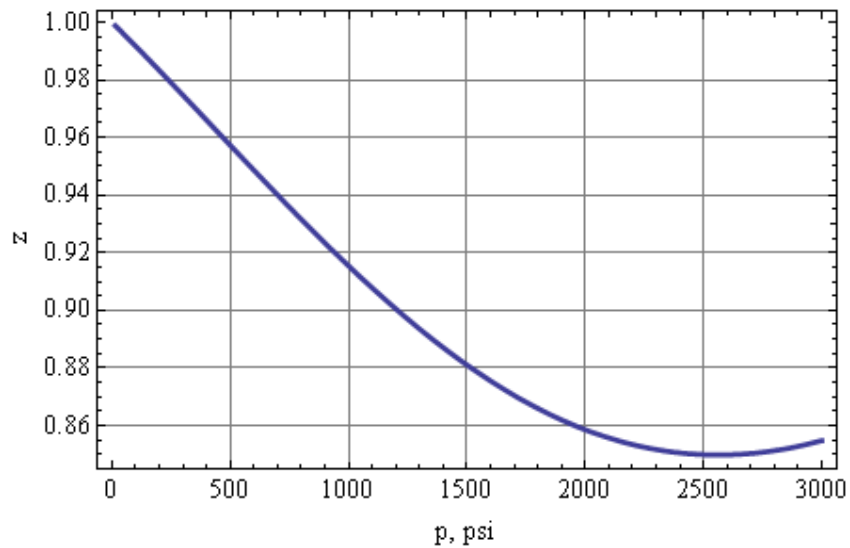
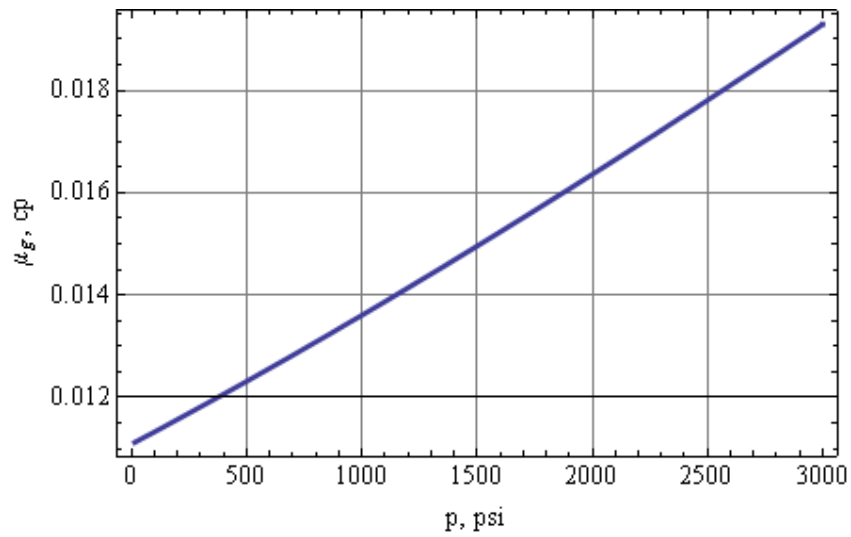Fig E1: Compressibility Factor vs. Pressure

Fig E2: Viscosity vs. Pressure

Fig E2 shows Gas Viscosity vs. Pressure. Gas viscosity correlation given by Carr, Kobayashi, and Burrows (1954) has been used which is a two step procedure to calculate gas viscosity. First we calculated the gas viscosity at given temperature and atmospheric pressure using gas gravity and inorganic compound composition and then corrected the viscosity to actual pressure by using a correlation.
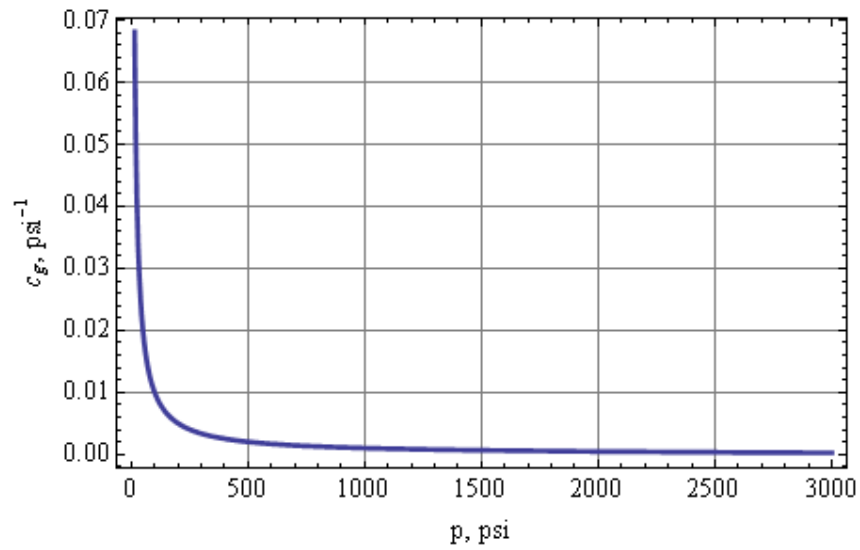
Fig E3: Gas Compressibility vs. Pressure

Fig E3 is for Gas Compressibility vs. Pressure. Gas compressibility is the measure of relative volume change of gas in response to the pressure change. Equation E-1 can be used to calculate Gas Compressibility at any temperature and pressure.

$$C_g = -\frac{1}{V}\left(\frac{\partial V}{\partial p}\right)_T = \frac{1}{p} - \frac{1}{z}\frac{\partial z}{\partial p}$$
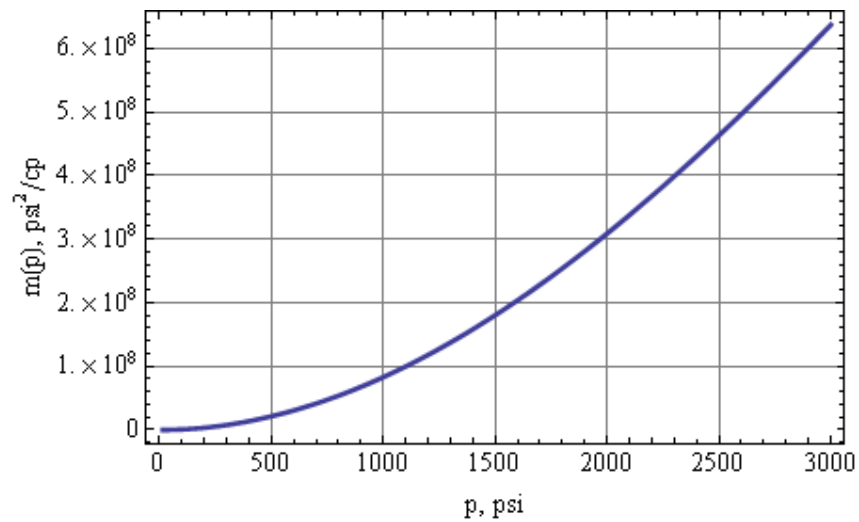
Fig E4: Real Gas Pseudo Pressure Plot

Fig E4 is real gas pseudo pressure plot. Real gas pseudo pressure is defined as

$$m(p) = \int_{P_b}^{p} \frac{2p}{\mu z} dp$$

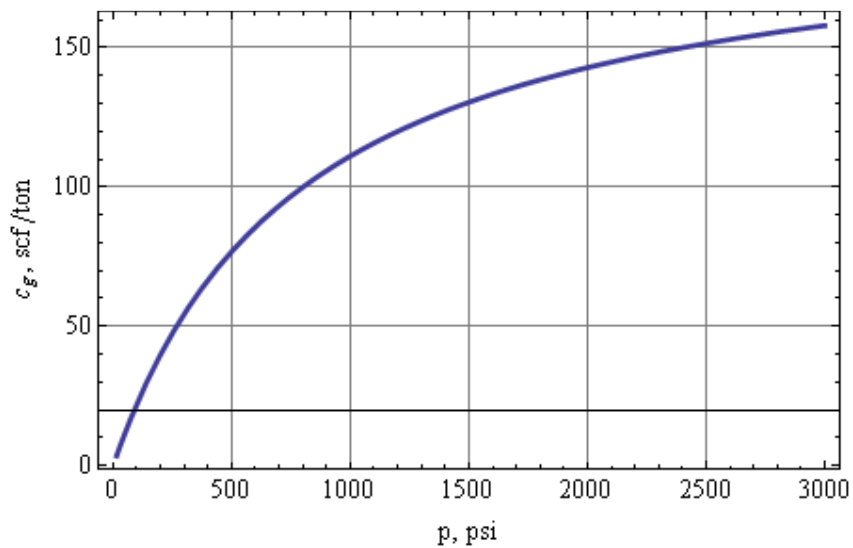Numerical integration was performed to calculate the pseudo-pressure.

Fig E5: Standard cubic feet of Adsorbed Gas per Tons of Rock vs. Pressure

Fig E5 gives us standard cubic feet of adsorbed gas per ton of rock mass vs. Pressure. Since this model has been developed for being used in gas shale reservoir where gas is stored on rock surface by adsorption this information is required. The desorbed gas volume should be included in material balance calculation. Well known, Langmuir type equation was used for this calculation.

Langmuir Type Isotherm Equation:

$$V_e = \frac{V_L P}{P_L + P}$$

where V_e is adsorbed gas content (gas volume per unit mass of rock), p is gas pressure, V_L is Langmuir volume that represents the maximum gas storage capacity of the rock, P_L is the Langmuir pressure and its equal to gas pressure at which rock adsorbs the gas volume equal to half of its maximum capacity. The above equation is based on mono-layer concept (Type I isotherm) so it's only valid for low pressure and where the pore sizes are equal to gas molecule size.

At high pressure gas desorption rate is low and the rate increases as the pressure goes down. So we expect adsorbed gas contribution in production at late time of well life when reservoir pressure reduces to a significantly low value.

VITA

Name: Amrendra Kumar

Permanent Address: Harold Vance Department of Petroleum Engineering
                            Richardson Building (corner of Spence and Ross Streets), 3116
                            TAMU, College Station, TX 77843-3116 (USA)

E-mail Address: amrendra7548@gmail.com

Education: Texas A&M University, College Station, Texas, USA

                            Master of Science in Petroleum Engineering

                            December 2008

                            Indian School of Mines, Dhanbad, India

                            Bachelor of Technology in Petroleum Engineering

                            May 2003

Affiliations: Society of Petroleum Engineers